SAFETY PROFILE AND PREVENTION OF COGNITIVE DEFICIT IN ALZHEIMER'S DISEASE MODEL OF GRAPHENE FAMILY NANOMATERIALS, TUCUMA OIL (*Astrocaryum vulgare*) AND ITS SYNERGISMS

Patricia Ferreira Schopf[a&]; Mikaela Peglow Pinz[b&]; Ketlyn Pereira da Motta[b]; Vitor Pereira Klein[c]; Alencar Kolinski Machado[a]; Cristiano Rodrigo Bohn Rhoden[a]; Ethel Antunes Wilhelm[b]; Cristiane Luchese[b*]; Ivana Zanella[a]; Michele Rorato Sagrillo[a*]

[&] Equal contribution

[a] Postgraduate Program in Nanosciences, Franciscan University, CEP 97010-032 Santa Maria, RS, Brazil

[b] Graduate Program in Biochemistry and Bioprospecting, Laboratory of Biochemical Pharmacology (LaFarBio), Center for Chemical, Pharmaceutical and Food Sciences (CCQFA), Federal University of Pelotas (UFPel), CEP 96010-900 Pelotas, RS, Brazil

[c] Biomedicine Course, Franciscan University, CEP 97010-032 Santa Maria, RS, Brazil

* Corresponding authors

Michele Rorato Sagrillo: Programa de Pós-graduação em Nanociências, Universidade Franciscana, Santa Maria, CEP 97010-032, RS, Brazil; E-mail: sagrillorm18@gmail.com; Phone: 55-55-32201200

Abstract

Alzheimer's disease is a worldwide health issue, and there are currently no treatments that can stop this disease. Oxidized graphene derivatives have gained prominence in use in biological systems due to their excellent physical-chemical characteristics, biocompatibility and ability to overcome the blood-brain barrier. Other substances highlighted are those of natural origin from the Amazon biome, such as tucuma, a fruit whose oil has been widely studied in therapeutic applications. Thus, the aim of this study was to investigate the action of graphene oxide, reduced graphene oxide and tucuma oil, isolated and combined, as an alternative for treatment of Alzheimer's disease through studies in silico, in vitro, in vivo and ex vivo. Computational simulation via docking was used to verify the affinity of the substances with the proteins β-amyloid and acetylcholinesterase, in which the reduced graphene oxide was the one that showed the most favorable interaction. The results of the ab initio simulation showed that the synergism between the nanostructures and the oil occurs through physical adsorption. The experimental results revealed that the substances and their combinations were nontoxic, both at the cellular and systemic level. In general, all treatments had positive results against induced memory deficit, but reduced graphene oxide was the most prominent, as it was able to protect against memory damage in all behavioral tests performed, with anticholinesterase activity and antioxidant effect. In conclusion, the reduced graphene oxide is, among the treatments studied, the one with great therapeutic potential to be investigated in the treatment of this disease.

Keywords: cell viability, computational simulations, graphene oxide, nanotoxicology, reduced graphene oxide, memory.

1. Introduction

Recently, carbon derived nanocompounds has emerged as a nanomaterial with numerous potential applications in the most diverse areas (Fraczek-Szczypta et al., 2018). Graphene can be defined as a monolayer of carbon atoms with sp^2 hybridization, having a honeycomb-like shape (Georgakilas et al., 2015). This nanostructure has excellent electrical, thermal and mechanical properties, being the thinnest and strongest material known until now (Chen et al., 2012). Despite these unique characteristics, graphene tends to aggregate and is extremely hydrophobic, limiting its use in biological systems (Reina et al., 2017et; Servant et al., 2014). In this context, hydrophilic nanomaterials derived from graphene, such as graphene oxide (GO) and reduced graphene oxide (rGO), arise as a potential alternative for biomedical applications (Viana et al., 2019; Mendonça et al., 2016).

From the oxidation and chemical exfoliation of graphite, graphene oxide (GO) is obtained, a process in which some carbon atoms with sp^2 hybridization are converted to sp^3 hybridization through the addition of oxygenated groups (Salles et al., 2020). The presence of these oxygenated functional groups makes the GO surface more electronegative, turning unique and completely different properties from other allotropic carbon materials and giving to GO an insulating character (Singh et al., 2018). To increase the conductivity, reduction reactions on this material can be performed, obtaining its reduced form i.e. rGO (Dreyer et al., 2010). rGO has a smaller number of oxygenated functional groups when compared to GO, which gives good electrical, thermal and mechanical conductivity, similar to graphene, although with high dispersion capacity in aqueous solutions, analogous its oxidated form (Dreyer et al., 2010). Recent studies have concluded that rGO is able to pass through the blood brain barrier (BBB) leaving it temporarily open, with no apparent toxicity to the organism (Mendonça et al., 2015). Mendonça and collaborators also demonstrated that the rGO managed to reach the hippocampus, which is one of the places most affected by Alzheimer's disease (AD) (Nobili et al., 2017). In addition, there is evidence that both rGO and GO can be applied as substrates in tissue engineering, highlighting the application of these nanostructures to support neural regeneration (He et al., 2016; Reddy et al., 2018; Shin et al., 2016). These indications point out that GO and rGO can be a promising tool to treat neurodegenerative diseases. Despite the excellent properties, issues related to the toxicity of carbon nanomaterials still do not have a consensus (Bianco, 2013; Guo & Mei, 2014).

Substances of natural origin have also attracted a lot of interest, as is the case with tucuma (*Astrocaryum vulgare*). Tucuma is a native fruit of the Amazon biome that has great nutritional relevance (Yuyama et al., 2008). From the pulp, an orange oil rich in properties can be extracted and used in several applications, such as in the production of edible oil, soap, cosmetics and herbal medicines (Shanley; Serra; Medina, 2010). This oil consists of 74.4% unsaturated fatty acids and 25.6% saturated fatty acids (Aguiar, 1996). Among these fatty acids are predominantly oleic acid (ω9), palmitic acid, linolenic acid (ω3), stearic acid and linoleic acid (ω6), respectively (Nascimento et al., 2019; Baldissera et al., 2017).

Expressive amounts of carotenes have also been identified in tucuma oil (TO), mainly *beta*-carotene (De Rosso; Mercadante, 2007; Ferreira et al., 2008; Yuyama et al., 2008). Furthermore, in the oil extracted from the tucuma relays the highest concentrations of *beta*-carotene when compared to the other parts of this fruit (Ferreira et al., 2008). Carotenoids are precursors of vitamin A, so TO is an important source of this vitamin (Nascimento et al., 2019). In addition to its excellent nutritional consistency TO can be considered an excellent natural antioxidant and anti-inflammatory (Bony et al., 2012). Baldissera et al. (2017) also demonstrate the hypoglycemic effect of TO in a model of diabetes, where there was an improvement in insulin levels in the body. In this context, the oil extracted from the tucuma can represent a potential effect on human health and a possible alternative for the use in the treatment of various diseases that cause oxidative stress, however, the toxicological profile of this substance needs to be most studied.

AD is the most common form of dementia that currently affects more than 40 million people worldwide and is among the epidemic trends for the coming years due to population aging (Poirier; Gauthier, 2016). AD remains unresolved, although there are treatments aimed at improving the quality of life. These treatments consist in the use of drugs that improve cognition and delay brain degeneration, nevertheless, causing adverse and toxic effects to the body with no reverse the brain damage already caused by the disease (Masoumi et al., 2018). One of the major challenges related to the treatment of AD, as well as other neurodegenerative diseases, is the administration of substances that manage to pass through the BBB (Serlin et al., 2015). In this sense, the use of graphene-derived nanostructures as carriers of the bioactive substances in TO can be a promising treatment alternative.

In this way, firstly we attempted to elucidate how nanomaterial and TO interact with proteins involved in the AD through an *in silico* and cytotoxicity *in vitro* study. Furthermore, another purpose of this study was to examine the effect of nanomaterial (GO and rGO) and TO, isolated and/or combined, in learning and memory impairment in a sporadic Alzheimer's disease model in mice, as well as the mechanisms involved in their pharmacological actions. Finally, we investigated if the treatments may cause cytotoxicity, even as renal and hepatic damage in mice.

2. Materials and Methods

2.1 In silico experiments

2.1.1 First Principles Simulation

The molecular structures used for GO and rGO were based on the model by Rosas et al. (2011). The 3D molecules of the major structures of TO were obtained from the PubChem website (Wang et al., 2016). To evaluate the energetic, structural and electronic properties of the major structures of TO (ω9, ω3, ω6, palmitic acid, stearic acid, retinoic acid and *beta*-carotene) interacting with graphene oxide and reduced graphene oxide the SIESTA program (Spanish Initiative for Electronic Simulations with Thousands of Atoms) was used (Soler et al., 2002), which is based on the density functional theory (DFT) using self-consistent Kohn-Sham equations and the local density approximation (LDA) to describe the exchange and correlation potential. In all simulations, a double base ζ plus a polarized function (DZP) was used. The binding energies were calculated using the following expression:

$$E = (E_{nano+oil}) - E_{nano} - E_{oil}$$

Where, E is the binding energy given in eV, $E_{nano+oil}$ is the total energy of the system, E_{nano} is the energy of the isolated nanostructure (GO or rGO) and E_{oil} is the energy of the isolated TO component. Afterwards, the electronic properties were analyzed through the difference between the highest occupied molecular orbital (HOMO) and lowest unoccupied molecular orbital (LUMO). The value of the isosurface used for the load plot in HOMO and LUMO was 0,001 e⁻/Bohr³.

2.1.2 Molecular docking

The molecular docking procedure was performed to verify the interactions between β-amyloid (Aβ42) and acetylcholinesterase (AChE) proteins with GO, rGO, ω3, ω6, ω9, palmitic acid, retinoic acid and beta-carotene, as a preliminary study for the application of nanostructures and TO in the treatment of AD. The molecular structures of proteins were obtained from the Protein Data Bank (Aβ42 - PDB ID: 2BEG; AChE - PDB ID: 4EY6) (Bermam et al., 2000). The docking study was carried out using the AutoDock Vina® program (Trott; Onson, 2010). The center of the box for each protein was predicted using the DeepSite® software (freely available at www.playmolecule.org, accessed on 05 April 2021) (Jiménez et al., 2017). The dimensions for the docking box were previously determined according to Feinstein and Brylinski (2015). All coupling experiments were carried out with an exhaustivity parameter of 8 (Forli et al., 2016). The strength of the interactions is calculated from a free energy of binding (FEB), given in kcal/mol.

Atoms with a distance less than 7 Å were interacting atoms (Silveira et al., 2009). Docking is not favorable when the FEB is greater than or equal to 0 kcal/mol or when there is a complete lack of for the exchange and correlation term. Briefly, the verification of the conformation and structure of better affinity was given based on two criteria: (i) most negative FEB value; and (ii) root mean square deviation (RMSD) with a maximum value of 2 Å and different from zero (Durruthy et al., 2017). The more negative the FEB value, the stronger the receptor-ligand link will be. The RMSD measurement is used to test the accuracy of a docking method (Forli et al., 2016; Trott and Olson, 2010). The analysis of non-covalent intermolecular interactions of the macromolecule-ligand complex was performed using 2D diagrams automatically plotted by LigPlot v.4.5.3 (Laskowski; Swindells, 2011).

2.2 Chemicals

GO and rGO were obtained commercially from the Sigma-Aldrich®. For the cell culture experiment, the nanostructures were diluted in ultrapure water Milli-Q (Millipore Corporation®) (5 mg/mL) with the aid of ultrasonic bath. The TO was prepared at a concentration of 16000 μg/mL, where the oil was diluted in surfactants and ultrapure water under magnetic stirring and temperature of 40 °C, according to previous studies by the group (Nascimento et al., 2019). For the *in vivo* experiments, GO and GO were previously solubilized in distilled water (1 mg/mL). The TO was administered to animals in its pure form (10 ml/kg).

Streptozotocin (STZ) was obtained from Sigma (St. Louis, MO) and it was dissolved in sterile filtered water. All the other chemicals used in this experiment were of the highest purity and obtained from standard commercial suppliers.

2.3 In vitro experiments

2.3.1 Cell culture and treatments

HFF-1 human fibroblast cells (ATCC® SCRC-1041[TM]) were used, commercially acquired from the Rio de Janeiro Cell Bank. The cells were cultured in Dulbecco's Modified Eagle Medium (DMEM) (Sigma®), supplemented with 10% (v/v) inactivated fetal bovine serum (Sigma®) and 1% penicillin/streptomycin (Sigma®), in a humid atmosphere 5% de CO_2 at 37 °C. The medium was changed every 2 days and the cells were trypsinized when reaching 90% confluence. The concentration of 2×10^5 cells/mL was obtained by counting in Neubauer's chamber with Trypan blue dye (0.4%). The cells were maintained in 96-well microplates for a period of 24 h for fixation. The cytotoxicity of the treatments was evaluated for 24 h: GO and rGO (1, 3, 10, and 30 μg/mL), TO (10 μg/mL) (Nascimento et al., 2019) and GO or rGO (1, 3, 10, and 30 μg/mL) + TO (10 μg/mL) association, according to the laboratory protocol. The negative control of the experiment was constituted by cells and culture medium, and the positive control by cells, culture medium and hydrogen peroxide (10 μM) as a damage inducer. Table 1 shows the experimental groups of the *in vitro* study and their composition.

Table 1. Qualitative and quantitative composition of the experimental groups of the in vitro study.

Groups		Cells (μL)	Culture medium (μL)	Treatment (μL)	H_2O_2 (μL)
Treatmens	GO	50	130	20	-
	rGO	50	130	20	-
	TO	50	130	20	-
	GO or rGO +TO	50	110	20/20	-
Negative control		50	150	-	-
Positive control		50	100	-	50

2.3.2 Evaluation of cell viability

The cytotoxicity assay was performed using the MTT technique (3- (4,5-dimethylthiazol-2-yl) -2,5-diphenyl tetrazolium bromide), following the methodology described by Krishna et al. (2009). The MTT reagent (Sigma®) was dissolved in phosphate buffered saline (0.01 mol/L; pH 7.4; 5 mg/mL). 20 μL of this solution was added to each well, incubating for another 4 hours (37 °C and 5% CO_2). Afterwards, the plates were centrifuged, and the supernatant was removed so that there was no interference, especially with respect to the nanostructures. The cells were resuspended in dimethylsulfoxide (DMSO) (Sigma®). Absorbance was measured at 560 nm in an Elisa Anthos® 2010 plate reader (Labtec, Austria) and cell viability was expressed as a percentage of the negative control value. The experiment was carried out in triplicate.

2.4 In vivo experiments

2.4.1 Animals

Male adult Swiss mice (25–35 g) from the Federal University of Pelotas, Brazil were used in this study. The animals were maintained at a constant temperature (22 ± 1 ℃), on a 12 h dark/light cycle (with lights on at 6:00 a.m.), with free access to food and water. Animal care and all experimental procedures were conducted in accordance with the Committee on Care and Use of Experimental Animal Resources, Federal University of Pelotas, Brazil (CEEA 1974/2016) and in compliance with the National Institute of Health Guide for the Care and Use of Laboratory Animals (NIH publications no. 80-23, revised in 1996) (National Research Council, 1996). Every effort was made to minimize the number of animals used and their discomfort.

2.4.2. Experimental protocol

Mice were randomly divided into 10 experimental groups (6 animals/group) (Table 2). Thirty minutes before initiating induction, mice received the intragastrically (i.g.) treatments via gavage as described in Table 2. After treatments, mice belonging to the V, VI, VII, VIII, IX and X groups were induced with STZ (2 µL of 2.5 mg/ml solution, intracerebroventricular (i.c.v.)), while I, II, III and IV groups received saline solution (vehicle) (2 µL, i.c.v.). The i.c.v. infusions of STZ or saline were administered using a microsyringe with a 28-gauge, 3.0 mm long stainless-steel needle (Hamilton) according to a previous report (Haley and Mccormick, 1957, Fronza et al. 2019). STZ injected i.c.v. (glucosamine-nitrosourea compound) mimics AD in mice (Grieb 2016; Martini et al. 2019; Pinz et al. 2021). On the third day of experimental protocol, i.c.v. injections were repeated. All animals were anesthetized with isoflurane before i.c.v. injections. During the dissection of the animal brain, the success of the injection was examined macroscopically, discarding animals whose injection occurred in an inappropriate place or caused cerebral hemorrhage.

Experimental Mice received treatments by i.g. route every day, until the tenth day of the experimental protocol. On the ninth day of experimental protocol, behavioral tests were initiated. An observer blinded to the study plan performed all observations. On the eighteenth day, mice were anaesthetized by inhalation of isoflurane for blood collection by cardiac puncture. Later, livers, kidneys and brains were removed for *ex vivo* experiments. The experimental protocol is demonstrated in Fig.1.

Table 2. Experimental groups.

Group	Treatment
I – Sham	Distilled water 10 mL/kg (i.g.) + Saline (i.c.v.)
II – GO	GO 1 mg/kg (i.g.) + Saline (i.c.v.)
III - rGO	rGO 1mg/kg (i.g.) + Saline (i.c.v.)
IV – TO	TO 10 mL/kg (i.g.) + Saline (i.c.v.)

V – STZ	Distilled water 10 mL/kg (i.g.) + STZ (i.c.v.)
VI - GO+STZ	GO 1 mg/kg (i.g.) + STZ (i.c.v.)
VII - rGO+STZ	rGO 1 mg/kg (i.g.) + STZ (i.c.v.)
VIII - TO+STZ	TO 10 mL/kg (i.g.) + STZ (i.c.v.)
IX - GO+TO+STZ	GO 1 mg/kg (i.g.) + TO 10 mL/kg (i.g.) +STZ (i.c.v.)
X - rGO+TO+STZ	rGO 1 mg/kg (i.g.) + TO 10 mL/kg (i.g.) +STZ (i.c.v.)

Animals were treated intragastrically (i.g.) with graphene oxide (GO), reduced graphene oxide (rGO), tucuma oil (TO) and distilled water 30 minutes before intracerebroventricular (i.c.v.) streptozotocin (STZ) or i.c.v. saline infusion. On day three of the experimental protocol, the i.c.v. induction with STZ or saline was repeated. The i.g. treatments were performed every day, until the seventeenth day of the experimental protocol. The number of mice tested was 6 each group.
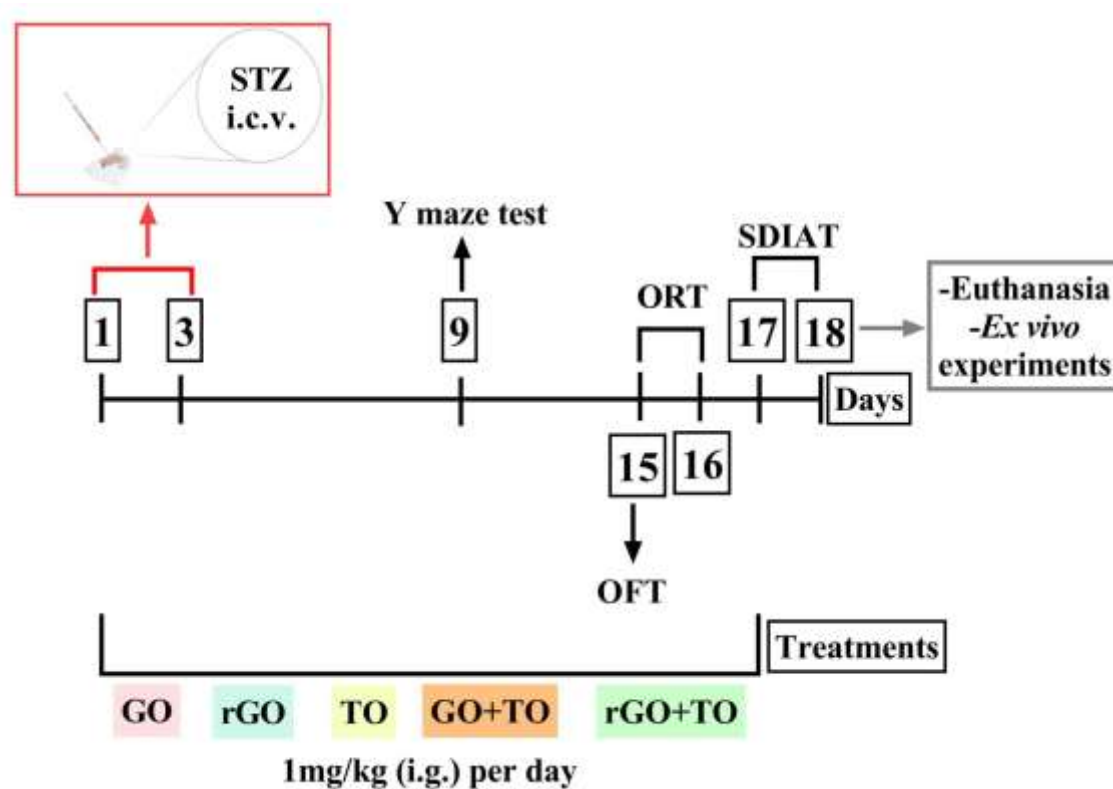

Fig. 1. Scheme of experimental protocol. Thirty minutes after intragastric (i.g.) treatments, mice received streptozotocin (STZ) or vehicle (saline) intracerebroventricularly (i.c.v.). On day three of the experimental protocol the i.c.v. injections were repeated. The i.g. treatments were performed every day, until the seventeenth day of the experimental protocol. Behavioral tasks started on the nine day of the experimental protocol. On the ninth day the Y-maze task was performed. On the fifteenth day the open-field test (OFT)

and object recognition task (ORT) was performed. On the sixteenth day ORT was performed. On the seventeenth and eighteenth days the step-down inhibitory avoidance task (SDIAT) was performed. On the eighteenth day, after the SDIAT test, the mice were sacrificed.

2.4.2 Behavioral tests
2.4.2.1 Open field test (OFT)

The OFT was carried out to identify locomotors disabilities, which might influence other tasks. This test evaluated the spontaneous locomotor and exploratory behaviors of mice (Walsh and Cummins, 1976). The OFT apparatus was made of plywood and surrounded by 30 cm-high walls. The floor of the open-field (40 cm long × 40 cm wide) was divided into 9 squares (3 rows of 3). Each animal was placed at the center of the open field and observed for 4 min to record the locomotor (number of segments crossed with the four paws) and exploratory (number of readings on the hind limbs) activities. The OFT test was performed on the fifteenth day of experimental protocol (Fig. 1).

2.4.2.2 Y-maze task

The Y-maze task was performed as described by Sarter et al. (1988) and it was used as a measure of working memory. The Y-maze apparatus consisted of a three-arm horizontal maze (40 cm long and 3 cm wide with walls 12 cm high) in which the three arms at 120° angles to each other, radiated out from a central point. The Y-maze task was performed on the ninth day of experimental protocol (Fig. 1). Mice were initially placed within one arm (A), and the arm entry sequence (e.g. ABCCAB, where letters indicate arm codes) and the number of arm entries were recorded manually for each mouse over an 8 min period. Alternation was determined from successive entries into the three arms on overlapping triplet sets in which three different arms are entered. An actual alternation was defined as entries into all three arms consecutively (i.e. ABC, CAB or BCA but not BAB). An entry was defined as placing all four paws within the boundaries of the arm.

2.4.2.3 Object recognition tasks

ORT was used to assess the short-term (STM) and long-term (LTM) memories of mice. ORT was performed in an open-field apparatus according to Stangherlin et al. (2009). On the day of the task (fifteenth day of experimental protocol) (Fig. 1), each animal was submitted to a habituation session in the absence of objects for 5 min. Subsequently, four objects were used: A1, A2, B and C. All objects were made of plastic, measuring 10 x 10 cm (length x height). During the training, on the fifteenth day of the experimental protocol, the animals were placed in the arena containing two identical objects (objects A1 and A2) for 5 min. Exploration was defined when the animal directed its nose within 2 cm of the object while looking, sniffing, or touching it. The STM of mice was evaluated 1.5 h after training in the presence of a familiar object (A1) and a new object (B), and the total time spent in exploring each object was determined during 5 min to measure the learning and recognition memory. The LTM was performed 24 h after training, on the sixteenth day of the experimental protocol, where mice were placed to explore a familiar object (A1) and a new object (C) for 5 min and the total time spent in exploring each object was determined. Data were expressed as a percentage of the exploratory preference and calculated as follows:

$$IR = \left(\frac{A2}{(A1 + A2)}\right) \times 100$$

$$STM = \left(\frac{B}{(A1 + B)}\right) \times 100$$

$$LTM = \left(\frac{C}{(A1 + C)}\right) \times 100$$

2.4.2.4 Step-down inhibitory avoidance task (SDIAT)

SDIAT was performed to evaluate aversive and non-spatial LTM as described by Sakaguchi et al (2006). During the training session (on the seventeenth day of the experimental protocol) (Fig. 1), each mouse was placed on the platform. When it stepped down and placed its four paws on the grid floor, an electric shock (0.5 mA) was delivered for 2 s. Twenty-four hours after the training session, the mice were tested under the same conditions without electric shock. Each mouse was placed again on the platform, and the transfer latency time (i.e., time taken to step down from the platform) (seconds) was measured as in the training session. The maximum transfer latency time (seconds) was 300 s.

2.5 Ex vivo assays

2.5.1 Brain sample preparation

The cerebral cortices and hippocampus (n = 6 for each experimental group) were separated in order to submit each sample to all neurochemical determinations. The cerebral structures (cerebral cortices and hippocampus) were washed with cold saline solution (0.9 %). The samples were homogenized in 0.25 M sucrose buffer (1:10, w/v) to determine AChE activity and 50 mM Tris-HCl, (1:10, w/v) to determine thiobarbituric acid reactive (TBARS) and reactive species (RS) levels, and superoxide dismutase (SOD) activity. Thus, homogenates were centrifuged at 900 xg for 10 min at 4 °C to obtain supernatant fraction (S1).

2.5.2 AChE activity

The AChE enzymatic assay was performed according to the method of Ellman et al. (1961), with some modifications, using acetylthiocholine as substrate. The method is based on the formation of the yellow anion, 5-thio-2-nitro-benzoic acid, measured by absorbance at 412 nm during 2 min incubation. Results were expressed as µmol/(acetylthiocholine) AcSCh/h/mg protein.

2.5.3 SOD activity

The SOD activity was assayed spectrophotometrically as described by Misra and Fridovich (1972). This method is based on the capacity of SOD in inhibiting autoxidation of epinephrine to epinechrome. The color reaction was measured at 480 nm. Aliquots of S1 were added in a 50 mM sodium carbonate (Na$_2$CO$_3$) buffer pH 10.3 and the enzymatic reaction was initiated by adding epinephrine. One unit of enzyme was defined as the amount of enzyme required to inhibit the rate of epinephrine autoxidation by 50 % at 26 ºC. The enzymatic activity was expressed as units (U SOD)/mg protein.

2.5.4 RS levels

The RS quantification was determined by a spectrofluorimetric method, using 2′,7′-dichlorofluorescein diacetate (DCHF-DA) assay as described by Loetchutinat et al. (2005). The S1 was incubated with DCHF-DA (1 mM). The oxidation of DCHF-DA to fluorescent dichlorofluorescein (DCF) was measured for the detection of intracellular RS. The DCF fluorescence intensity emission was recorded at 520 nm (with 480 nm excitation), 15 min after the addition of DCHF-DA to the medium. The results were expressed as arbitrary units of fluorescence (UF).

2.5.5 TBARS levels

The lipid peroxidation was evaluated by TBARS formation (Ohkawa et al., 1979). An aliquot of S1 was added to the reaction mixture containing: thiobarbituric acid (0.8 %), sodium dodecyl sulfate (SDS) (8.1 %), and acetic acid (pH 3.4) and incubated at 95 °C for 2 h. The absorbance was measured at 532 nm. Results were expressed as nmol malondialdehyde (MDA) /mg protein.

2.5.6 Plasma glucose levels

Plasma glucose levels were determined to further confirm that 2 µL of 2.5 mg/mL of STZ is a subdiabetogenic dose.   After collection of heparinized blood, the samples were separated by centrifugation at 900 xg for 15 min and glucose levels were determined by an enzymatic colorimetric method using a commercial kit (Bioclin, Brazil). Glucose levels were expressed as mg/dL.

2.5.7 Toxicological analysis

Samples of livers and kidneys were collected and homogenized in 50 mM Tris/HCl pH 7.5, (1:10, w/v) and centrifuged at 900 xg for 10 min at 4 °C to yield S1. TBARS levels were assayed by the method of Ohkawa et al. (1979) described above (item 2.5.5). The RS levels were assayed by the method of Loetchutinat et al. (2005) described above (item 2.5.4). These dosages were determined for the evaluation of oxidative damage in the livers and kidneys of mice after treatments. Heparinized bloods were collected, and plasma samples were obtained by centrifugation at 900xg for 10 min and used for biochemical assays. Biochemical assays were performed using commercial kits. Alanine (ALT) and aspartate (AST) aminotransferase activities were used as biochemical markers for early acute hepatic damage, and they were determined by the colorimetric method (Reitman and Frankel, 1957). The values were expressed as U/l. Renal function was analyzed by determining plasma urea and creatinine (MacKay and MacKay, 1927). The values were expressed as mg/dL.

2.5.8 Protein determination

The protein concentration was measured by the Bradford method (1976), using bovine serum albumin as the standard.

2.6 Statistical analysis

The data are expressed as mean ± standard error of the mean (SEM). Data were analyzed by Graphpad Prism® 5 and the normality of data was evaluated by the D'Agostino and Pearson omnibus normality test.

Statistical analysis was performed using one-way ANOVA followed by the Newman-Keuls test. Values of $p < 0.05$ were considered statistically significant.

3. Results

3.1 In silico results

In Fig. 2 we show the active sites for the macromolecules Aβ42 and AChE and the respective sites where the simulation box was designed for the molecular docking study with the ligands. As can be observed in figure 2A, the Aβ42 protein receptor sites are located at a specific point in the macromolecule structure, whereas for AChE (Fig. 2C), the active sites are in a concentrated portion of its structure. From the coordinates obtained from the active sites, the structure of the simulation box was designed for both proteins (Fig. 2B and Fig 2D), with X = -8.7 Å, Y = 1.0 Å and Z = 0.7 Å for Aβ42 protein and X = 13.7 Å, Y = 43.9 Å and Z = 27.9 Å for AChE. Table 3 shows the box size for each of the binders. Table 3 shows the box size for each of the binders.
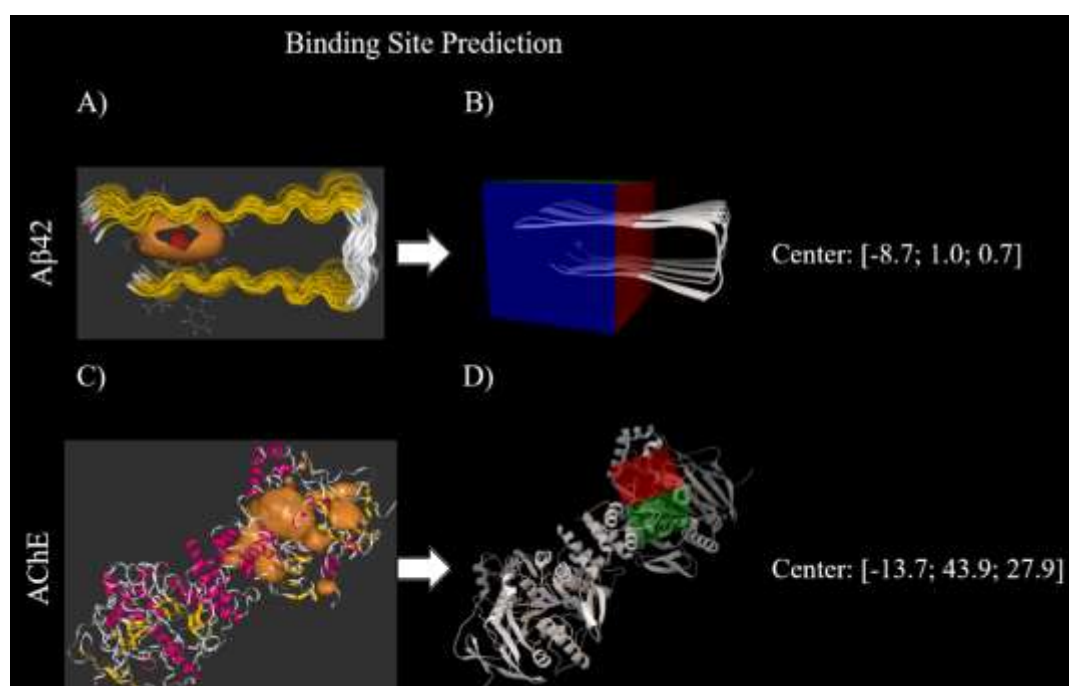

Fig. 2. (A) Representation of the predicted binding sites for β-amyloid protein (Aβ42). (B) Representation of the docking box simulation set for the most probable binding site of for β-amyloid protein (Aβ42) according with the maximum score in the DeepSite. (C) Representation of the predicted binding sites for acetylcholinesterase (AChE). (D) Representation of the docking box simulation set for the most probable binding site for acetylcholinesterase (AChE) according to the maximum score in the DeepSite.

Table 3. Docking box dimensions for each of the studied binders.

Ligand	Box dimensions (Å)
GO	(27.983; 27.983; 27.983)
rGO	(27.895; 27.895; 27.895)
ω3	(15.999; 15.999; 15.999)
ω6	(18.612; 18.612; 18.612)
ω9	(19.080; 19.080; 19.080)
Palmitic acid	(27.710; 27.710; 27.710)
Stearic acid	(31.076; 31.076; 31.076)
Retinoic acid	(21.750; 21.750; 21.750)
Beta-carotene	(42.835; 42.835; 42.835)

Afterward, molecular docking approaches were carried out to assess the interaction between protein binding and different ligands. Table 4 shows the values of free energy of binding or affinity (kcal/mol) obtained for the best docking complexes with values of RMSD <2 Å.

Table 4. Affinity and RMSD values obtained for the best fit configurations based on the free binding energy between the ligands and the β-amyloid (Aβ42) and acetylcholinesterase (AChE) proteins, highlighting the best affinity ligand with the symbol (*).

Ligand	Aβ42		AChE	
	Affinity (kcal/mol)	**RMSD (Å)**	**Affinity (kcal/mol)**	**RMSD (Å)**
GO	-13.7	1.077	-10.4	1.606
rGO*	-15.8	1.656	-11.9	1.834
ω3	-4.1	1.743	-7.0	1.344
ω6	-3.8	1.797	-6.6	1.479
ω9	-3.6	1.749	-6.4	1.211
Palmitic acid	-4.8	2.216	-6.0	1.551
Stearic acid	-4.5	1.188	-5.2	1.438
Retinoic acid	-6.2	1.495	-9.3	1.279
Beta-carotene	-7.4	1.531	-9.9	1.402

Figure 3 shows the types of interactions and the relevant target residues involved in docking between the protein Aβ42 and rGO, which was the system of greatest affinity among those studied.
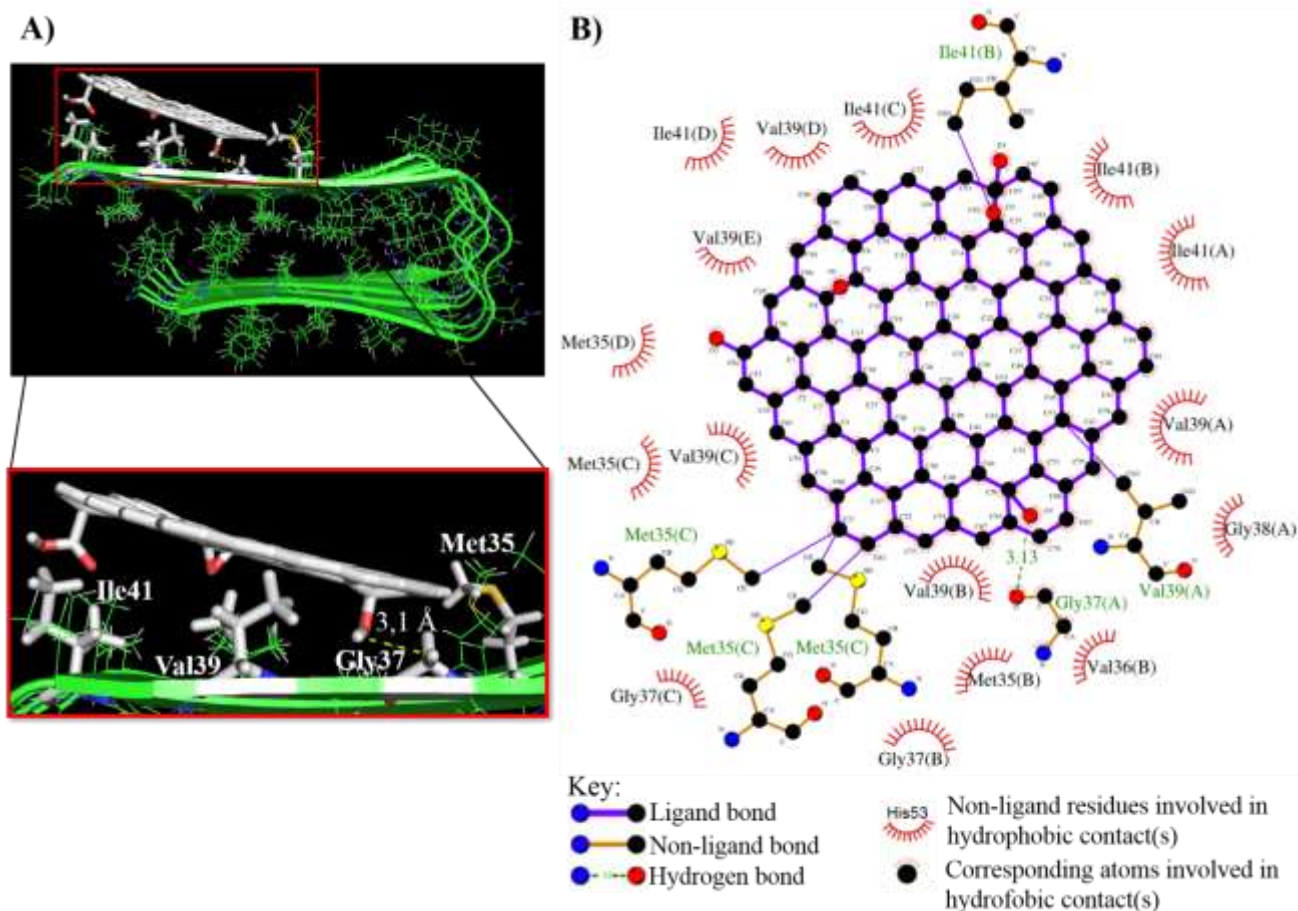

Fig. 3. Interaction between reduced graphene oxide (rGO) and β-amyloid protein (Aβ42): (A) representation of the best fit configuration and (B) 2D diagram of the types of interactions involved in the system.

The interactions and the relevant target residues involved between the rGO and AChE complex were also analyzed. Figure 4 shows the diagram of the interactions of this system.
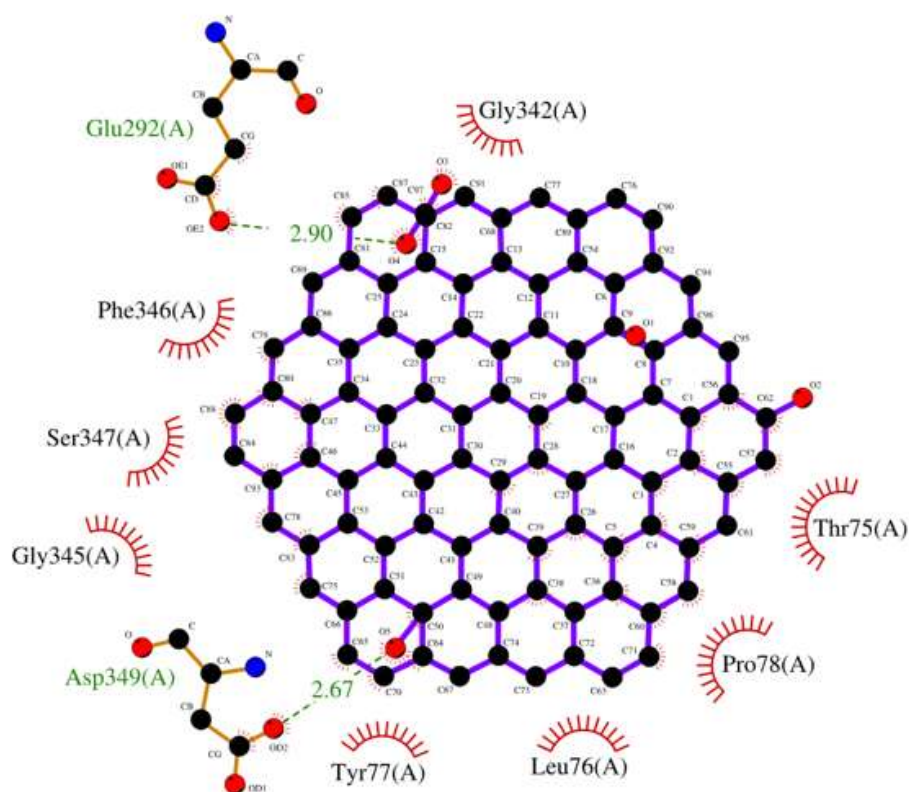
Fig. 4. 2D diagram of interactions between acetylcholinesterase (AChE) and reduced graphene oxide (rGO).

In addition to molecular docking studies, calculations of first principles were performed to assess the interaction between nanostructures (GO and rGO) and the major components of TO. Interactions were made in different arrangements between the molecules according to the most susceptible regions through the interactions observed in the analysis of the isolated molecules. Table 5 shows the values of the shortest distance between atoms, binding energy (Elig), difference HOMO-LUMO (ΔHL) and charge transfer (Δq) only for the most stable configurations of GO/rGO+TO systems. The images of the molecular structures optimized for each of these systems can be seen in Supplementary Material as Fig. S1.

Table 5. Initial distance, final distance, binding energy (E_{lig}), difference HOMO-LUMO (ΔHL) and charge tranfer from tucuma oil components (TO) to nanostructures (Δq) for graphene oxide (GO)/reduced graphene oxide (rGO) + major components of TO.

System	Initical distance (Å)	Final distance (Å)	E_{lig} (eV)	ΔHL (eV)	Δq (e^-)
GO+palmitic acid	2.00 (H_{61}-H_{157})	1.45 (H_{134}-H_{139})	-2.05	0.18	+0.04
GO+stearic acid	2.00 (H_{61}-H_{156})	1.70 (H_{137}-H_{185})	-1.76	0.16	+0.25
GO+ω3	2.00 (H_{61}-H_{178})	1.95 (H_{137}-H_{172})	-2.28	0.16	+0.18
GO+ω6	2.00 (H_{135}-H_{183})	1.56 (H_{134}-H_{138})	-1.77	0.14	+0.06
GO+ω9	**2.00 (H_{137}-H_{176})**	**1.27 (H_{58}-O_{139})**	**-2.87**	**0,13**	**+0,03**
GO+retinoic acid	2,00 (H_{137}-H_{165})	1,85 (H_{61}-H_{180})	-2,26	0,17	+0,14
GO+beta-carotene	2,00 (H_{61}-H_{227})	1,99 (H_{137}-H_{222})	-2,01	0,08	-0,13

rGO+palmitic acid	2.00 (C_{20}-H_{147})	2.54 (C_{65}-H_{173})	-1.28	0.10	+0.30
rGO+stearic acid	2.00 (C_{24}-H_{162})	2.30 (H_{120}-H_{130})	-1.43	0.11	+0.31
rGO+ω3	2.00 (C_{20}-H_{173})	1.90 (H_{58}-H_{177})	-1.59	0.09	+0.33
rGO+ω6	2.00 (C_{22}-H_{169})	2.07 (H_{58}-H_{175})	-1.35	0.09	+0.33
rGO+ω9	**2.00 (C_{27}-H_{161})**	**1.29 (H_{58}-O_{130})**	**-2.20**	**0.07**	**+0.06**
rGO+retinoic acid	2.00 (C_4-H_{155})	1.30 (H_{58}-O_{130})	-1.86	0.02	+0.04
rGO+beta-carotene	2.00 (H_{120}-H_{191})	1.99 (H_{120}-H_{191})	-1.57	0.06	-0.09

Figure 5 shows the energy levels and the electronic charge distribution for the GO+ω9 (Fig. 5A) and rGO+ω9 interactions (Fig. 5B), which were the most stable.
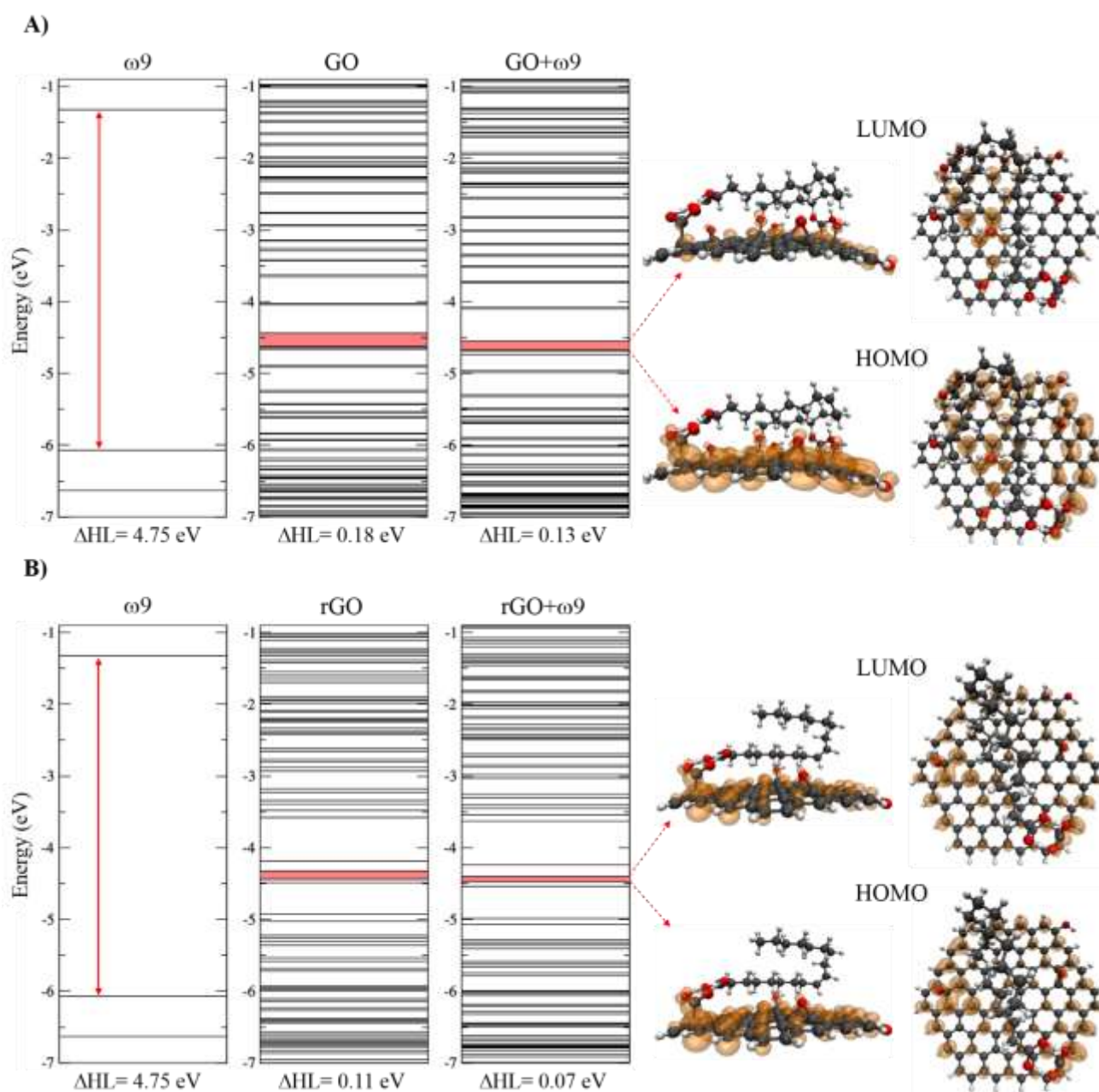

Fig. 5. Energy levels and local charge density for systems A) graphene oxide+ω9 (GO+ω9) and B) reduced graphene oxide+ω9 (rGO+ ω9).

3.1 Cytotoxicity

The effects of GO are isolated and combined with TO on the cell viability of fibroblasts shown in figure 6. The treatment of cells with GO for a period of 24 hours showed that this nanostructure did not affect cell viability in any of the tested concentrations (1, 3, 10, 30 mg/mL), being statistically equal to the negative control (CN) (CN: 100%; [1]: 109.40%; [3]: 119.11%; [10]: 100.31%; [30]: 89.93%) (Fig. 6A). The association of TO with GO also did not cause cell death and all tested concentrations were shown to be proliferative (Fig. 6B). In addition, it can be noted that there is no significant difference in cell viability between the tested concentrations ([1]: 134.19%; [3]: 142.92%; [10]: 158.97%; [30]: 149.14%). The positive control consisting of hydrogen peroxide at 10 μM, which was the damage pattern used in the test, showed low cell viability, around 50%.
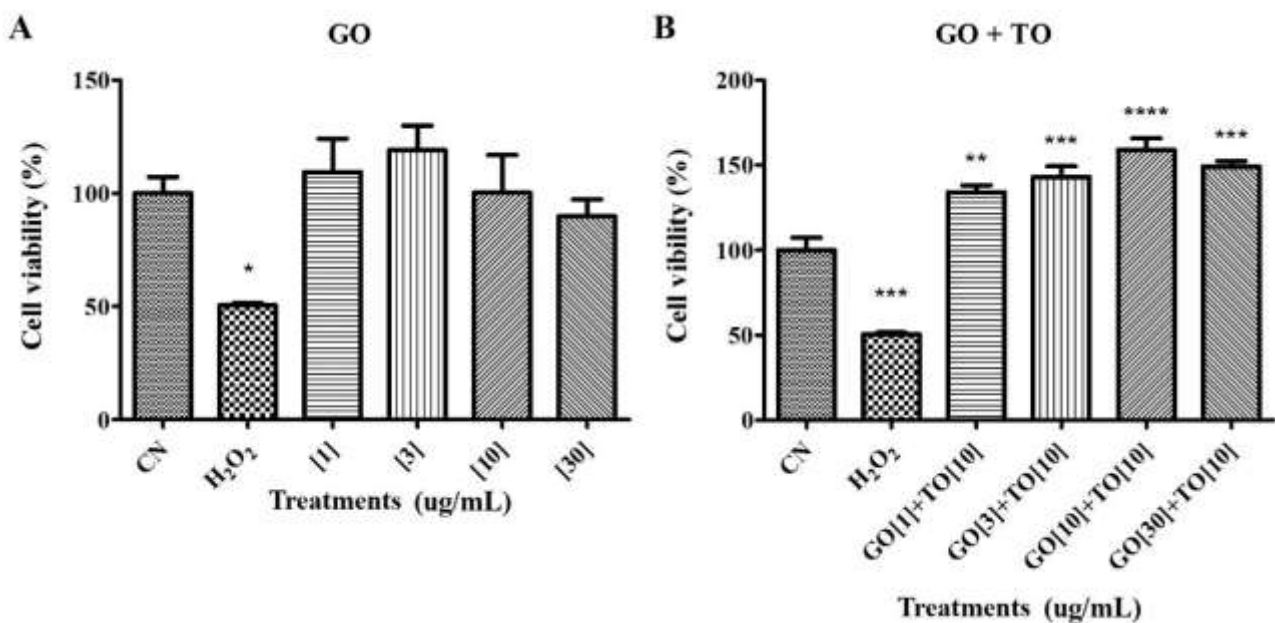

Fig. 6. Effect of graphene oxide (GO) (A) and synergism between graphene oxide (GO) and tucuma oil (TO) (B) on the viability of human fibroblast cells by reducing MTT within 24 hours of incubation. Results expressed as percentage of the negative control (100%). Data were expressed as mean ± standard error of the mean (SEM). Analyzes were performed by one-way ANOVA followed by Dunnett's test (n=3). Values with $p < 0.05$ were considered statistically significant, being * $p < 0.05$, ** $p < 0.01$ and *** $p < 0.001$.

The possible cytotoxic effects of treating cells with rGO alone and combined with TO were also investigated (Fig. 7). The results showed that treatment with rGO for a period of 24 hours did not affect cell viability at any of the tested concentrations (Fig. 7B). The concentration of 30 mg/mL demonstrated cell proliferation and there was no significant difference in relation to CN (CN: 100%; [1]: 100.14%; [3]: 92.55%; [10]: 94.57 %), indicating absence of cytotoxicity. The synergism of rGO with TO also did not cause cell death and all tested concentrations were shown to be proliferative, with no significant difference between them ([1]: 180.59%; [3]: 188.58%; [10]: 200.06%; [30]: 189.56%) (Fig. 7B).
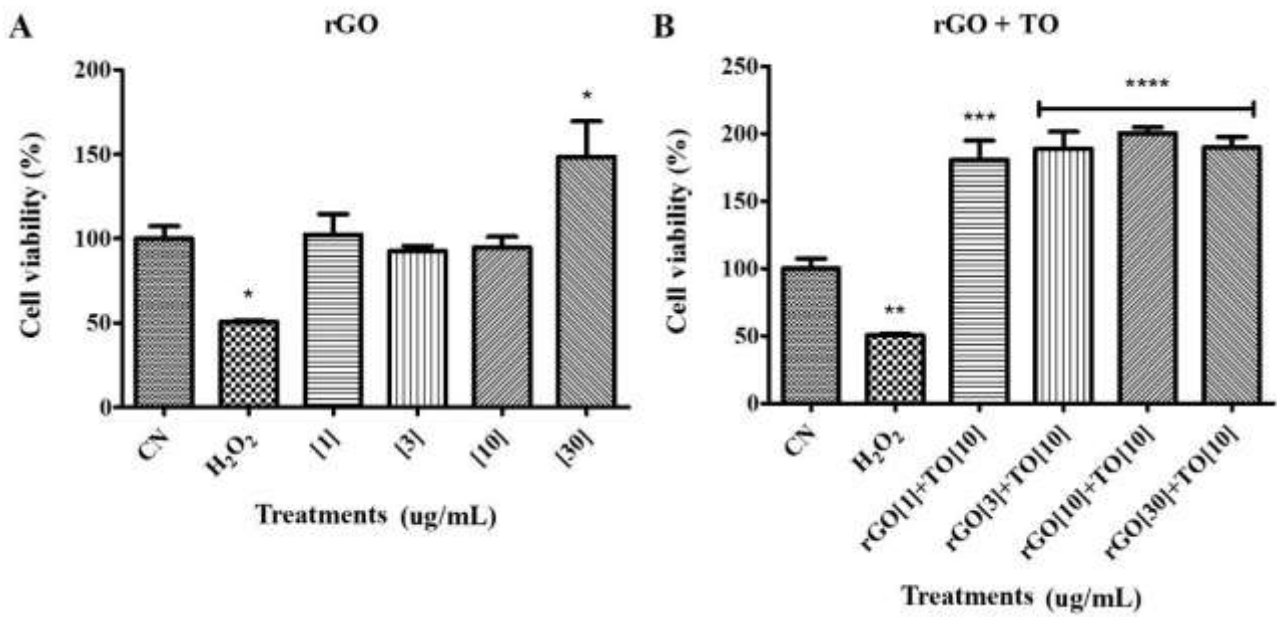
Fig. 7. Effect of reduced graphene oxide (rGO) (A) and synergism between reduced graphene oxide (rGO) and tucuma oil (TO) (B) on the viability of human fibroblast cells by reducing MTT within 24 hours of incubation. Results expressed as percentage of the negative control (100%). Data were expressed as mean ± standard error of the mean (SEM). Analyzes were performed by one-way ANOVA followed by Dunnett's test (n=3). Values with $p < 0.05$ were considered statistically significant, being * $p < 0.05$, ** $p < 0.01$ and *** $p < 0.001$.

3.2 In vivo experiments
3.2.1 GO, rGO, TO and STZ did not cause any significant change in locomotor and exploratory activities

The one-way ANOVA followed by Newman-Keul's test demonstrated that treatments did not cause any significant change in the number of rearings (ANOVA: $F_{9,50} = 2.184$, p= 0.0390) or crossings (ANOVA: $F_{9,50} = 0.6109$, p= 0.4744) (Fig. 8A and Fig. 8B).
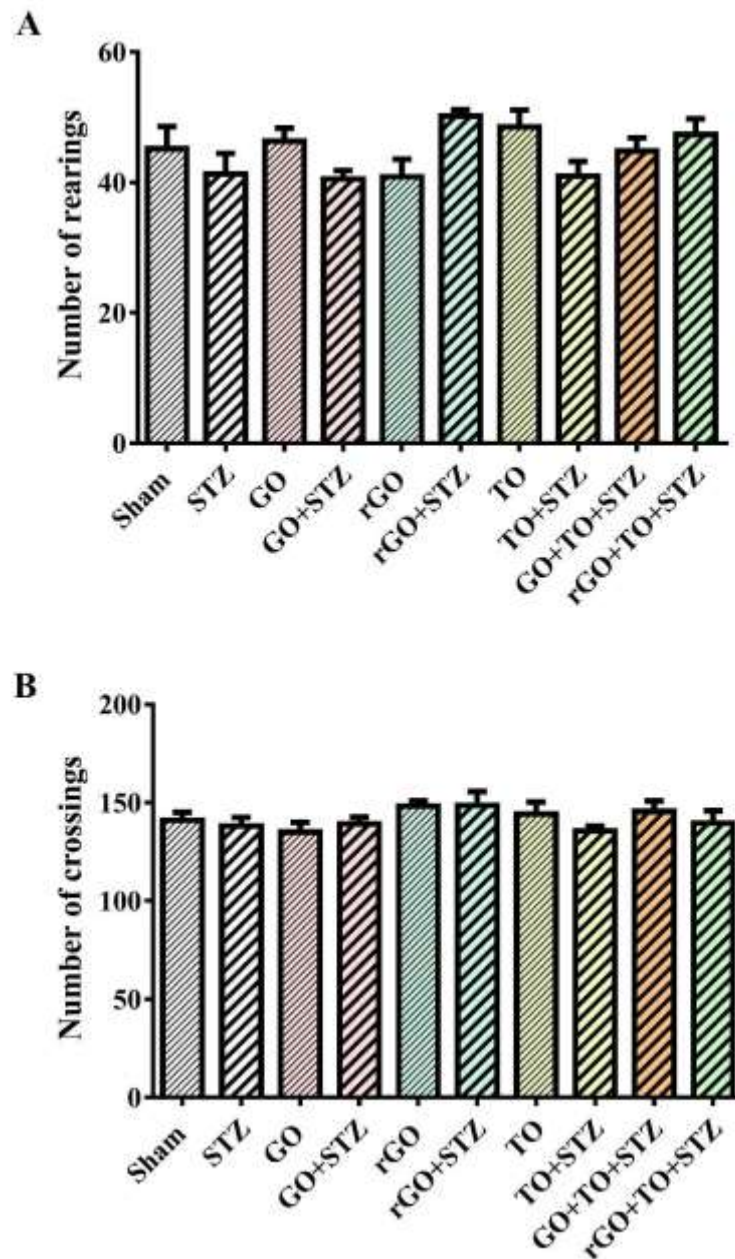
Fig. 8. Effect of graphene oxide (GO), reduced graphene oxide (rGO), tucuma oil (TO) isolated and combined, and/or streptozotocin (STZ) on the open-field test (OFT) on the (8A) number of rearings and (8B) number of crossings. Data are reported as mean ± standard error of the mean (SEM) of six animals per group (one-way analysis of variance/Newman-Keuls test).

3.2.2 GO, rGO and TO protect against cognitive and memory impairment induced by i.c.v. injections of STZ

The one-way ANOVA followed by Newman-Keul's test demonstrated that STZ reduced the spontaneous alternation behavior in the Y-maze task, when compared with the Sham group (Fig. 9A). GO, rGO and TO, prevented the reduction of spontaneous alternation behavior, when compared with the STZ group (ANOVA: $F_{9, 50} = 5.114$, $p < 0.0001$) (Fig. 9A). Also, synergisms of GO+TO and rGO+TO, prevented the reduction of spontaneous alternation behavior, when compared with the STZ group, but did not cause

any significant change when compared to their respective groups (GO+STZ, rGO+STZ and TO+STZ) (Fig. 9A). The treatments did not cause any significant change in the number of arm entries (ANOVA: $F_{9,50}$ = 0.984, p= 0.4648) (Fig. 9B) in the Y-maze task.

The one-way ANOVA followed by Newman-Keul's test revealed that there was no difference in the exploratory preference of objects among groups in the training phase (ANOVA: $F_{9,50}$ = 0.9968, p= 0.4549) (Fig. 9C) in the ORT. STZ reduced the exploratory preference of the new object in the STM (Fig. 9D) and LTM (Fig. 9E), when compared with the Sham group. Treatments with GO, rGO and TO were able to prevent these reductions in the STM (Fig. 9D) and LTM (Fig. 9E), when compared with the STZ group (ANOVA: $F_{9,50}$ = 2.421, p= 0.0228 for STM; ANOVA: $F_{9,50}$ = 3.254, p= 0,0035 for LTM) in the ORT. Also, synergisms of GO+TO and rGO+TO, prevented the reduction in the exploratory preference of the new object in the STM (Fig. 9D) and LTM (Fig. 9E), when compared with the STZ group, but did not cause any significant change when compared to their respective groups (GO+STZ, rGO+STZ and TO+STZ groups) (Fig. 9D and Fig. 9E).

In the training phase of SDIAT, there was no difference in the transfer latency time among groups (ANOVA: $F_{9,\,50}$ = 2.072, p= 0.0502) (Fig. 9F). In the test phase, STZ decreased the transfer latency time, when compared with the Sham group (Fig. 9F). GO, rGO and TO treatments significantly prevented this reduction (ANOVA: $F_{9,50}$ = 8.172, p<0.0001), when compared with the STZ group (Fig. 9G). Synergism of GO+TO did not prevent the reduction in the transfer latency time, while synergism rGO+TO had effect in preventing this parameter, when compared with the STZ group (Fig. 9F). Also, synergism rGO+TO did not cause any significant change when compared with rGO+STZ and TO+STZ groups, but synergism of GO+TO was different when compared with GO+STZ and TO+STZ groups (Fig. 9F).
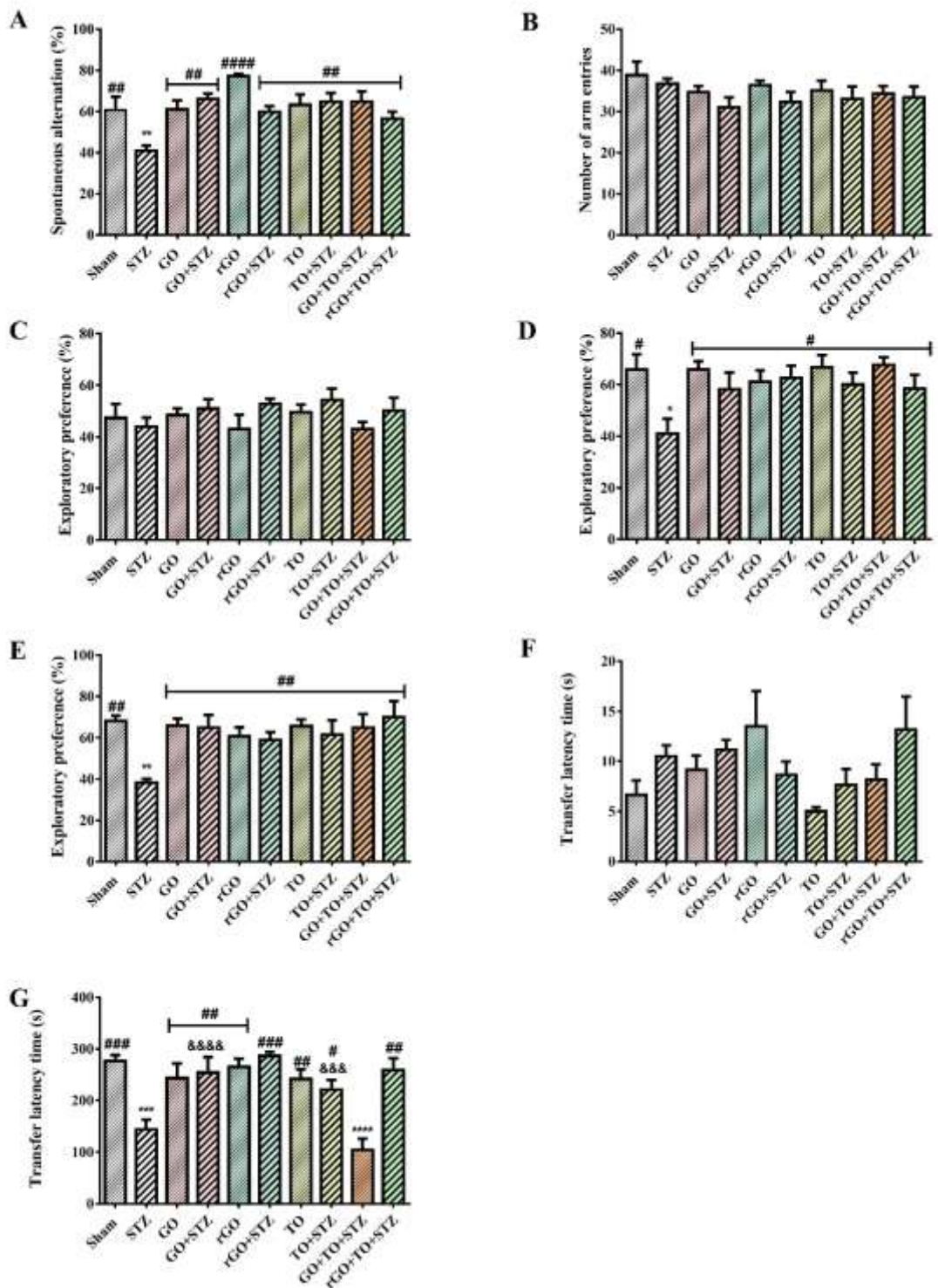
Fig. 9 Effect of graphene oxide (GO), reduced graphene oxide (rGO), tucuma oil (TO), isolated and combined and/or streptozotocin (STZ) on the memory and cognition tests of mice. Spontaneous alternation behavior (9A) and number of arm entries (9B) in the Y-maze task; training (9C), first trial (percentage of time spent exploring the novel object, test carried out 1.5 h after training) (9D) and second trial (percentage of time spent exploring the novel object, test carried out 24 h after training) (9E) in the object recognition task (ORT); training (latency (s) to fall from the platform) (9F) and test (latency (s) to fall from the platform) (9G) in the step-down inhibitory avoidance task (SDIAT). Data are reported as mean ± standard error of the mean (SEM) of six animals per group (one-way analysis of variance/ Newman-Keul's test). (*) p <

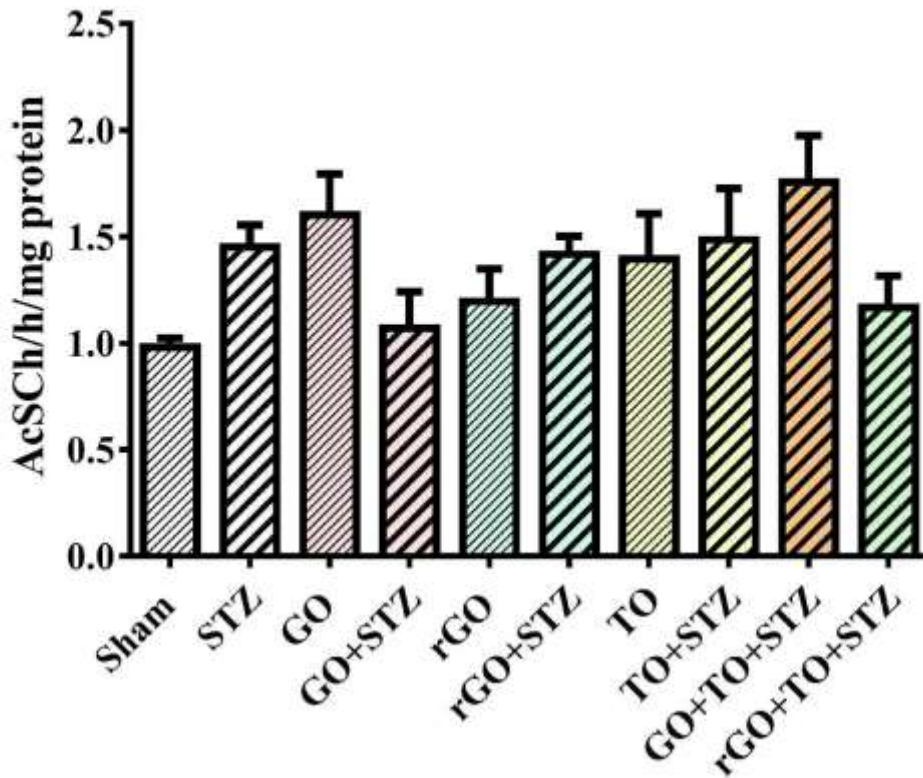0.05, (**) p < 0.01, (***) p < 0.001 as compared with the sham group. (#) p < 0.05, (##), p < 0.01, (###), p < 0.001, (####), p < 0.0001 as compared with the STZ group. (&&&), p < 0.001, (&&&&), p < 0.0001 as compared with the GO+TO+STZ group.

3.2.3 rGO and TO treatments protects against increase in AChE activity induced by i.c.v. injections of STZ

Figure 10A demonstrated that no alteration was observed in the AChE activity in the cerebral cortices of mice (ANOVA: $F_{9,50} = 2.092$, p= 0.0480).

STZ administration promoted a significant increase in the AChE activity in the hippocampus of mice, when compared with the Sham group (Fig. 10B). rGO and TO treatments, but not GO treatment, significantly prevented the increase in the AChE activity caused by STZ in the hippocampus of mice (ANOVA: $F_{9,50} = 8.551$, p<0.0001) (Fig. 10B). Synergism of GO+TO did not prevent the increase in the hippocampus AChE activity, while synergism rGO+TO had effect in preventing this parameter, when compared with the STZ group (Fig. 10B). Also, synergism rGO+TO did not cause any significant change when compared with rGO+STZ and TO+STZ groups, but synergism of GO+TO was statistically different from TO+STZ group and similar to GO+STZ group (Fig. 10B).
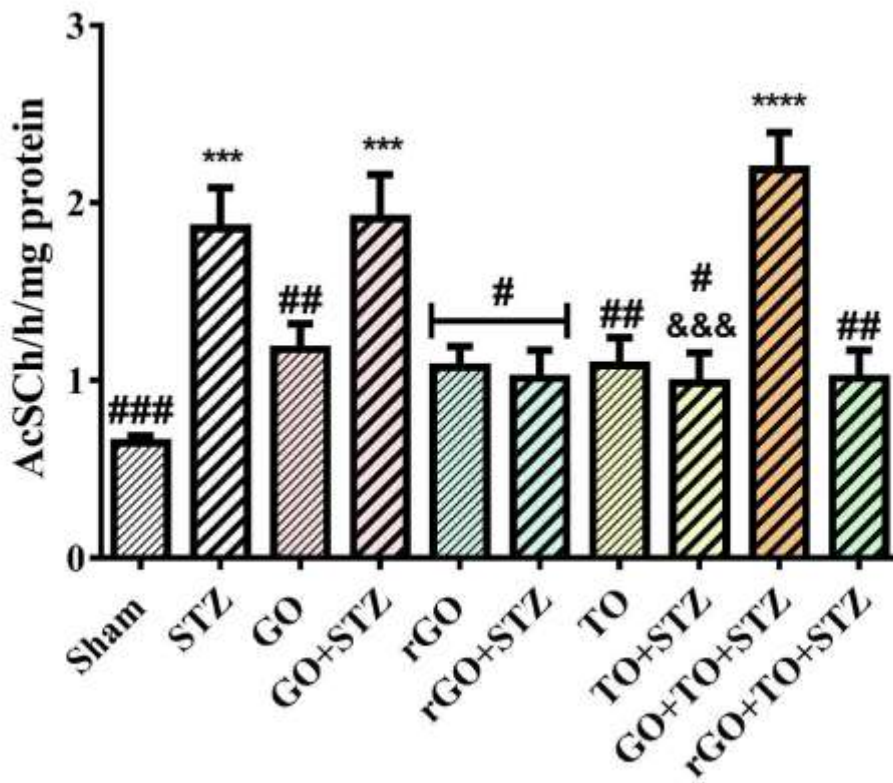
A

B

Fig. 10 Effect of graphene oxide (GO), reduced graphene oxide (rGO), tucuma oil (TO) isolated and combined, and/or streptozotocin (STZ) on the acetylcholinesterase (AChE) activity in cerebral cortex (10A) and hippocampus (10B) of mice. Data are reported as mean ± standard error of the mean (SEM) of six animals per group (one-way analysis of variance/ Newman-Keul's test). (*) $p < 0.05$, (**) $p < 0.01$, (***) $p < 0.001$ as compared with the sham group. (#) $p < 0.05$, (##) $p < 0.01$, (###) $p < 0.001$ as compared with the STZ group. (&&&) $p < 0.001$ as compared with the GO+TO+STZ group.

3.2.4 GO, rGO and TO treatments modulates oxidative stress induced by i.c.v. injections of STZ

STZ administration promoted a significant increase in RS levels in the cerebral cortices (Fig.11A) and hippocampus (Fig.11B) of mice, when compared with the Sham group. GO and TO treatments significantly prevented the increase of RS levels caused by STZ in the cerebral cortices (ANOVA: $F_{9,50} = 2.64$, p= 0.0139) (Fig. 11A). Synergism of rGO+TO did not prevent the increase in the RS levels, while synergism GO+TO had effect in preventing this parameter, when compared with the STZ group (Fig. 11A). Also, synergisms did not cause any significant change when compared to their respective groups (GO+STZ, rGO+STZ and TO+STZ groups) in the cerebral cortices of mice (Fig. 11A). Figure 11B showed that rGO treatment significantly prevented the increase of RS levels caused by STZ in the hippocampus, while GO and TO did not have effect (ANOVA: $F_{9,50} = 2.092$, p= 0.0480). Synergism GO+TO and rGO+TO, caused a significant decrease in the RS levels in the hippocampus of mice, when compared with the STZ group, but did not cause any significant change when compared to their respective groups (GO+STZ, rGO+STZ and TO+STZ groups) in the hippocampus of mice (Fig. 11B).

For TBARS levels, the one-way ANOVA followed by Newman-Keul's test showed that STZ increased the TBARS levels in the cerebral cortices (Fig. 11C) and hippocampus (Fig. 11D) of mice, when compared with the Sham group. The treatments with GO, rGO and TO reduce the STZ -induced increase in the TBARS levels in the cerebral cortices (ANOVA: $F_{9, 50} = 2.794$, p= 0.0098) (Fig. 11C). Synergism GO+TO and rGO+TO, caused a significant decrease in the TBARS levels in the cerebral cortices of mice, when compared with the STZ group, but did not cause any significant change when compared to their respective groups (GO+STZ, rGO+STZ and TO+STZ groups) (Fig. 11C). GO, rGO and TO did not reduce the STZ-induced increase in the TBARS levels in the hippocampus (ANOVA: $F_{9, 50} = 3.841$, p= 0.0010) of mice (Fig. 11D). Synergisms GO+TO and rGO+TO cause a significant decreased in the TBARS levels, when compared with the STZ group in the hippocampus of mice although did not cause any significant change when compared to their respective groups (GO+STZ, rGO+STZ and TO+STZ groups) (Fig. 11D).

Figure 11E demonstrated that no alteration was observed in the SOD activity in the cerebral cortices of mice (ANOVA: $F_{9, 50} = 2.079$, p= 0.0494). Figure 11F showed that STZ increased the SOD activity in the hippocampus of mice, when compared with the Sham group. GO, rGO and TO treatments significantly prevented the increase in hippocampus SOD activity induced by STZ (ANOVA: $F_{9,48} = 3.128$, p= 0.0048) (Fig. 11F). Synergism GO+TO and rGO+TO, caused a significant decrease in the SOD activity in the hippocampus of mice, when compared with the STZ group, but did not cause any significant change when compared to their respective groups (GO+STZ, rGO+STZ and TO+STZ groups) (Fig. 11F).
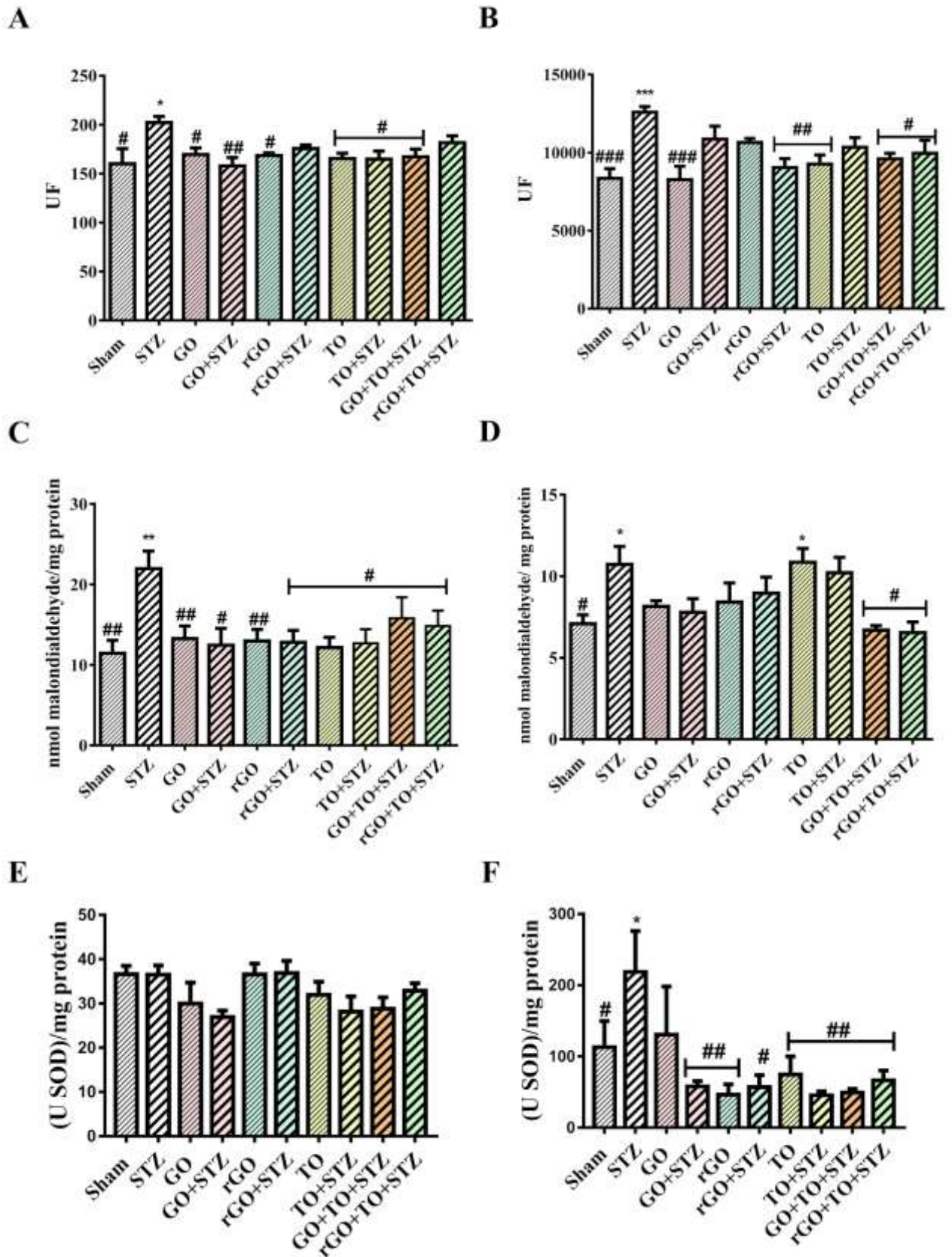
Fig. 11 Effect of graphene oxide (GO), reduced graphene oxide (rGO), tucuma oil (TO) isolated and combined, and/or streptozotocin (STZ) on the oxidative stress. Reactive species (RS) levels in cerebral cortex (11A) and hippocampus (11B) of mice. Thiobarbituric acid reactive species (TBARS) levels in cerebral cortex (11C) and hippocampus (11D) of mice. Superoxide dismutase (SOD) activity on cerebral

cortex (11E) and hippocampus (11F) of mice. Data are reported as mean ± standard error of the mean (SEM) of five-six animals per group (Due to lack of hippocampi samples in GO and rGO+STZ groups to SOD test) (one-way analysis of variance/ Newman-Keul's test) (*) $p < 0.05$, (**) $p < 0.01$, (***) $p < 0.001$, (****) $p < 0.0001$, as compared with the sham group. (#) $p < 0.05$, (##) $p < 0.01$, (###) $p < 0.001$, (####) $p < 0.0001$ as compared with the STZ group.

3.2.5 GO, rGO and TO treatments did not induce toxicity

The oral administrations of *GO, rGO and TO* (1 mg/kg/per day) did not cause death of exposed mice. In table 6, administrations of GO, rGO and TO did not alter ALT (ANOVA: $F_{9,48} = 0.6437$, p =0.7541) and AST (ANOVA: $F_{9,50} = 0.4774$, p =0.8829) activities, as well as urea (ANOVA: $F_{9,50} = 1.165$, p= 0.3377) and creatinine (ANOVA: $F_{9,49} = 0.8642$, p =0.5626) levels. Additionally, no alteration was observed in the RS and TBARS levels in the liver (ANOVA: $F_{9,50} = 1.412$, p= 0.2083 and ANOVA: $F_{9,50} = 1.095$, p= 0.3833, respectively) (Fig. 12A and Fig. 12B, respectively) and kidney (ANOVA: $F_{9, 50} = 0.7364$, p= 0.6738 and ANOVA: $F_{9, 50} = 0.4455$, p= 0.9033, respectively) (Fig. 12C and Fig. 12D, respectively) of mice, when compared to the control group.

Table 6. Effect of graphene oxide (GO), reduced graphene oxide (rGO), tucuma oil (TO) and/or streptozotocin (STZ) on the plasma biochemical markers in mice.

Group	AST (U/L)	ALT (U/L)	Urea (mg/dL)	Creatinine (mg/dL)
Sham	229.2 ± 18.08	96.7 ± 7.78	70.60 ± 4.60	0.40 ± 0.04
STZ	230.2 ± 23	94.3 ± 6.13	73.1 ± 3.11	0.45 ± 0.03
GO	206.2 ± 23	98.3 ± 5.06	71.6 ± 2.91	0.46 ± 0.02
GO+STZ	204 ± 10.47	96.1 ± 5.25	74.6 ± 4.55	0.39 ± 0.02
rGO	203.2 ± 23.28	94.3 ± 9.34	64.6 ± 3.85	0.42 ± 0.03
rGO+STZ	225.6 ± 12.48	99.8 ± 7.19	71.1 ± 2.65	0.42 ± 0.02
TO	197.8 ± 10.38	82.1 ± 3.98	67.4 ± 1.98	0.39 ± 0.04

TO+STZ	225.5 ± 24.22	88.8 ± 6.61	63.6 ± 3.55	0.47 ± 0.03
GO+TO+STZ	216.1 ± 16.91	92.5 ± 6.19	69.6 ± 3.06	0.41 ± 0.03
rGO+TO+STZ	232.6 ± 21.95	92.5 ± 7.37	65.1 ± 3.77	0.38 ± 0.02

Data are reported as mean ± standard error of the mean (SEM) of six animals per group. Statistical analysis was performed using one-way ANOVA followed by the Newman-Keuls test. *Abbreviations:* Aspartate (AST) and alanine (ALT) aminotransferases.
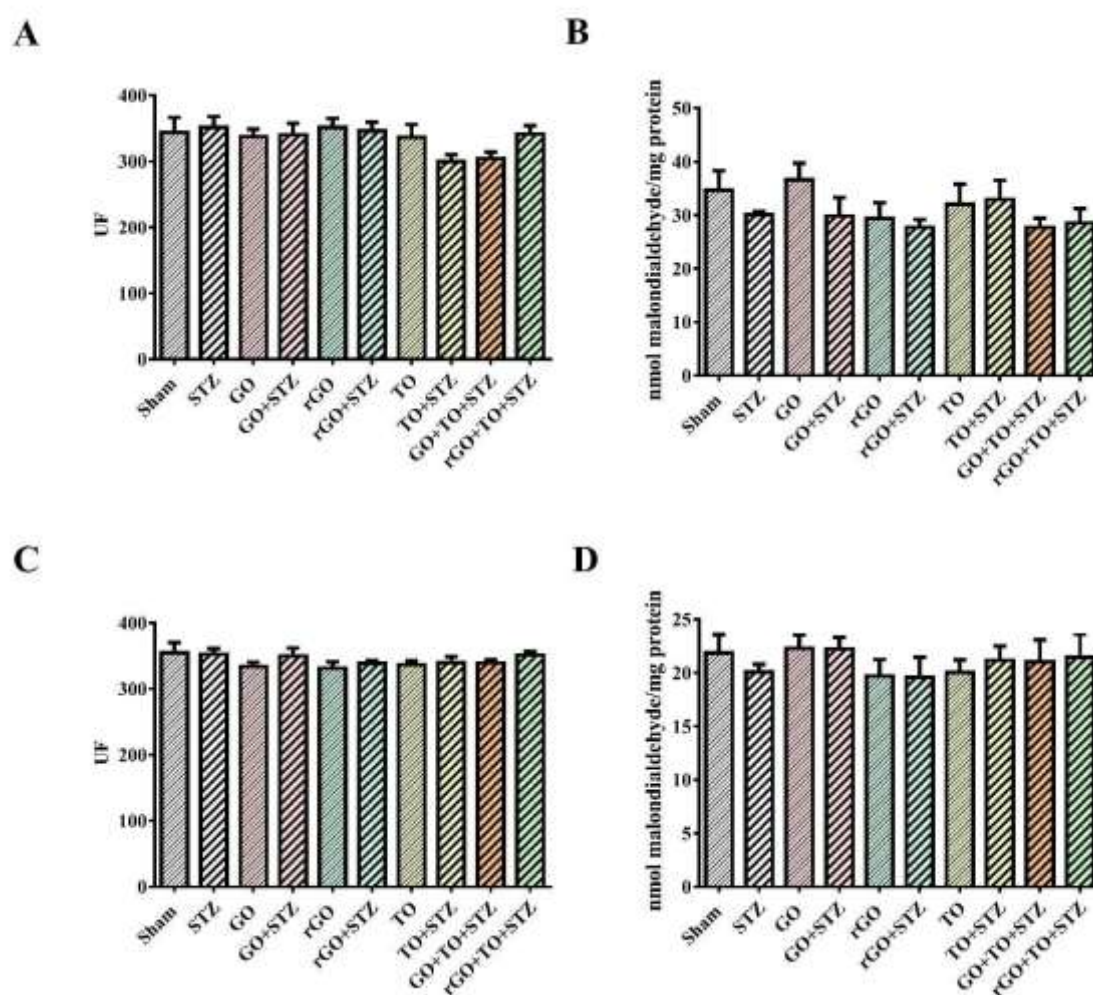

Fig. 12 Effect of graphene oxide (GO), reduced graphene oxide (rGO), tucuma oil (TO) isolated and combined, and/or streptozotocin (STZ) on the toxicity parameters. Reactive species (RS) levels in liver (12A) and kidney (12C) of mice. Thiobarbituric acid reactive species (TBARS) levels in liver (12B) and kidney (12D) of mice. Data are reported as mean ± standard error of the mean (SEM) of five-six animals per group (one-way analysis of variance/ Newman-Keul's test).

4. Discussion

In this study we showed, for the first time, through *in silico*, *in vitro*, *in vivo* and *ex vivo* analyses with GO, rGO and TO isolated and in synergism to verify the safety of use as well as the effectiveness of these substances in the treatment of mice submitted to the model of dementia sporadic Alzheimer's type induced with STZ. This study provided evidence that GO, rGO and TO are not cytotoxic and protected against STZ-induced learning and memory impairment, which was accompanied by modulation of AChE activity and oxidative damage in the brain structures of mice. Moreover, no changes were observed in plasma markers of kidney and liver damage, in addition to oxidative markers in these tissues.

Initially, a computer simulation study was carried out to evaluate the molecular mechanisms of interaction of GO, rGO and TO with biomolecules related to AD. In addition, the effects of synergism between nanostructures and major components of TO were also investigated. In fact, computer simulation in studies with nanomaterials is highly relevant, since the low dimensionality of these structures generates quantum effects that can be predicted *in silico*. Computational methods are a potential alternative to significantly reduce the use of animals, in addition to being a fast and low-cost method (Graham; Prescott, 2015; Passini et al., 2017).

Our results showed an interaction of nanostructures and major components of TO with protein Aβ42, demonstrating that all molecules had an affinity for the protein, except palmitic acid, which had an RMSD value higher than 2 Å. It was also possible to observe that GO and rGO showed an affinity greater than -13 kcal / mol, which indicates a high attraction of these nanostructures for protein Aβ42, with rGO being the substance with the best result. The fatty acids present in the TO were those that obtained the lowest affinity for the protein.

The best complexation between rGO and Aβ42 occurred through the interaction of the functional groups of the nanostructure with the amino acid's isoleucine, valine, glycine and methionine. The methionine amino acid residue is largely responsible for the toxicity of the peptide, so its interaction with the nanostructure is promising in the toxicity reduction (Varadarajan et al., 2001). It can also be noted that there was a 3.1 Å hydrogen bonding interaction between the glycine 37 of the protein A chain and the oxygen atom of the hydroxyl functional group of the nanostructure, which indicates a strong interaction between the protein and rGO. There is also a tendency for covalent bonding between isoleucine 41 in chain B and the oxygen atom of the carboxyl group, methionine 35 in chain C with carbons 63 and 71 and between valine 39 in chain A and carbon 53 in the nanostructure. In addition, there are weak interactions of the hydrophobic bond type between protein residues and rGO atoms. It is important to highlight that in a receptor-ligand complexation, a combination of strong and weak interactions occurs, which indicates that rGO, theoretically, has great possibilities to inhibit the Aβ42 protein.

The docking study was also carried out with the enzyme AChE, in which the highest values of affinity obtained were in interactions with the nanostructures. The molecule with the lowest affinity for the enzyme AChE was palmitic acid. The key active sites for AChE enzyme inhibition are tyrosine 337, histidine 447, glutamate 202 and serine 203 residues (Cheung et al., 2012). As can be seen, the AChE inhibitory drug interacts with these amino acids through hydrophobic interactions, with histidine 447, glutamate 202 and serine 203, and through hydrogen bonding with tyrosine 337, which is the main AChE

inhibitory site (Cheung et al., 2012). The rGO, despite having an extremely strong interaction with the enzyme (-11.9 kcal/mol) and presenting hydrogen bonds and hydrophobic interactions, does not interact with the fundamental enzyme inhibition residues known until today, and may act for some other type of mechanism still unknown.

In the docking study, it was observed that all the ligands analyzed had a good interaction for the protein Aβ42, and the rGO that showed the highest affinity for this protein. Although no experimental tests involving the Aβ protein have been performed, the simultaneous analysis of the theoretical and experimental results suggests that rGO has a great chance of acting on the Aβ protein and possibly reversing its activity in the brain, since this nanostructure was able to protect against the DA damage induced in mice in all *in vivo* tests performed and interacted with the main residue involved in the neurotoxicity of this protein *in silico* (Varadarajan et al., 2001).

Starting with the simulation of first principles, the most stable configuration found for the GO+TO system was with the GO interacting with ω9, since this system presented the highest binding energy in module (-2.87 eV). In this interaction, the charge transfer was 0.03 electrons and occurred from ω9 to GO. For the rGO+TO system, the most stable configuration was also observed in the interaction with the ω9 molecule, with - 2.20 eV binding energy and 0.06 electron charge transfer, occurring from ω9 to the nanostructure. These results indicate that both nanostructures in contact with TO interact preferentially with ω9. In the analysis of the energy levels of the most stable configurations, it is possible to notice that there is an overlap of the levels of ω9 with GO in the GO+ω9 interaction, as well as with ω9 and rGO in the rGO+ω9 interaction. The overlap in energy levels indicates that there is no change in the electronic properties of the systems in relation to the isolated structures, i.e., the properties of each of the structures are preserved in the interaction. The high binding energy of these systems observed in table 5 is related to the high number of interactions involved in the system, since there is a total contact of ω9 with the surface of the nanostructures. Evaluating the charge density plots of both interactions, we see a concentration of charges only in the nanostructures, both in LUMO and HOMO. Despite the image of the molecular structures of these interactions, apparently having a chemical bond between the carboxyl group of the nanostructures and the carboxyl group of ω9, there is no formation of this type of bond between the systems. The shortest distance found for the two systems is greater than 1.10 Å, which is one evidence for the lack of bindings. In addition, the concentration of charges in LUMO and HOMO in only one of the structures is a characteristic of the formation of physical bonds in these systems. Thereby, the results demonstrate that the systems preserve their own characteristics and there is weak interaction between the structures, characterized as physical adsorption type. Thus, the synergism of nanostructures with TO does not alter their intrinsic characteristics, and, furthermore, GO and rGO can be candidates that are considered promising for the transport of substances present in TO.

The MTT assay was performed to investigate whether the nanostructures isolated and combined with the TO have any cytotoxic effect on human fibroblast cells. These cells are located in tissues and organs throughout the body, so they are an important indicator for *in vitro* toxicity tests (Dick; Limaiem, 2019). In addition, considering the purpose of this study which is the administration of treatment orally. A non-invasive administration has advantages such as greater safety and convenience to the patient, where the fibroblasts would come into direct contact with the substances (Yildirimer et al., 2011). As defined in

ISO 10993-5 of 2009, which provides for *in vitro* cytotoxicity tests, a substance is considered cytotoxic when the result of *in vitro* tests has a cell viability of less than 75%. Based on the norm, the treatments with the nanostructures and their synergisms with the TO were not cytotoxic since they showed cell viability greater than 75%. However, treatment with rGO showed cell proliferation at a concentration of 30 mg/mL. This can be justified by the characteristic electrical conductivity of rGO allowing support for cell growth, since proliferation is influenced by the conductivity of its substrate (Reddy et al., 2018). As insulating nanomaterial, GO did not show this proliferative behavior in any of the tested concentrations. However, the synergism of GO and rGO with TO showed cell proliferation for all concentrations, indicating that the chemical matrix of TO has an influence on this obtained proliferation. This influence can be explained due to the presence of retinoic acid in the composition of the oil, since retinoids can regulate the expression of genes through different cell receptors, which are essential in inducing cell proliferation and differentiation (Baldissera et al., 2017). Based on the results obtained *in silico* and *in vitro* analyzes, we investigated the effect of GO, rGO and TO, as well as their synergisms, in a model of STZ-induced sporadic Alzheimer's disease in mice. As expected, STZ caused learning and memory impairment in animals, without changing blood glucose in accordance with Pinz et al. 2021. Indeed, we confirmed that STZ caused a loss of working memory, STM, LTM, and aversive memory and non-spatial LTM. Accordingly, memory and learning loss has been reported as the main symptom of Alzheimer's disease (Masoumi et al., 2018). Importantly, one of the main findings of this study was the protection of GO, rGO and TO against learning and memory impairment induced by STZ in mice. Except for aversive memory and non-spatial LTM (where treatment with GO+TO was harmful) the effects of synergism were not different from the effects of treatments alone in other types of memory. These findings need to be better elucidated with additional studies, considering that in the theoretical calculations of GO+TO synergism, no evidence was found to explain this behavior.

In this study, we observed that STZ caused an increase in the AChE activity in the hippocampus of mice. This result is supported by other relevant studies (Fronza et al. 2019; Martini et al. 2019). Importantly, we showed that GO, rGO and TO protected against the increase in the AChE activity. This result is of great importance, given that AChE terminates the cholinergic transmission by hydrolyzing acetylcholine (ACh). It is known AChE inhibitors are the most popular treatments for AD symptoms and these treatments aim to restore ACh neurotransmitter levels (Mokrani et al. 2019). Our results probably indicate that the modulation of AChE by GO, rGO and TO promotes an increase in ACh levels in the synaptic cleft of neurons, contributing to the improvement in memory and learning caused by these treatments. However, treatment with GO associated with TO increase the AChE activity. The exact mechanism to explain this increase remains unclear. This finding corroborates and explains the result observed in aversive memory and non-spatial LTM, but we were unable to xplain why synergism of GO + TO did not affect other behavioral tests. In addition, we suggested that the neurotransmitter ACh might play a more prominent role in this memory specifically. Synergism of rGO with TO was not different from the effects of treatments alone in AChE activity.

In order to investigate the mechanism in which GO, rGO and TO exert an effect to prevent behavioral changes caused by STZ, we studied the possible modulation of oxidative stress. In fact, oxidative damage has been implicated in the progression and pathogenesis of Alzheimer's disease (Butterfield and Halliwell 2019). In the present study, we proved that STZ caused an increase in the

oxidative stress in the cerebral structures of mice. We observed an increase in the RS levels and lipid peroxidation (as demonstrated by TBARS levels) induced by STZ in cerebral cortices and hippocampus of mice. Treatments with the nanostructures or TO, isolated or combined, presented a different effect depending on the analyzed cerebral structure. In the cerebral cortex, most treatments had an effect in reducing the RS levels and TBARS levels induced by STZ, except for combination from rGO together with TO, which had no protective effect on the RS levels in this cerebral structure. In the hippocampus, in general, the combinations, GO+TO and rGO+TO showed to be effective in reducing RS and TBARS levels. Regarding the isolated treatments, only rGO demonstrade an effect on the RS levels increased by STZ in the hippocampus of mice. Notwithstand the difficulty to explain the reasons for these differences, we can suggest that the effect of treatments, isolated or combined, in reducing oxidative damage may be related, at least in part, to their effect in improving the different types of memory studied.

SOD, another oxidative stress marker, is an enzyme responsible for biochemical processes in order to limit the impact of RS on essential cellular components. In this study, we believed that an increase in the SOD activity in the hippocampus occurred due to oxidative damage, as demonstrated by increase in the RS and TBARS levels, caused by STZ. All treatments, isolated or combined, normalized the SOD activity, probably by controlling the oxidative damage.

Concerning signs of hepatic and renal toxicity, GO, rGO, TO, isolated or combined, did not change plasma biochemical parameters and oxidative markers in these tissues. Hepatotoxicity is one of the main side effects found in the drugs available for the treatment of Alzheimer's disease, thereby the great relevance substances that treat this disease without this adverse effect on the body (Lima, 2008). These results of toxicity in mice agree with the results obtained *in vitro*, where treatments did not cause cytotoxicity. In addition, the absence of an unspecified behavior of GO, rGO, TO, isolated or combined, was proved in the OFT, since no animal showed alteration in the locomotor and exploratory activities.

5. Conclusion

In this study, we evaluated the molecular interaction *in silico*, the safety profile *in vitro* and *ex vivo* and the effects of GO, rGO and TO isolated and in synergism in the learning and memory impairment of mice submitted to a model of sporadic dementia induced with STZ. The results showed that the nanostructures showed a better interaction *in silico* with the protein β-amyloid and with AChE than the components of the oil, which in fact was observed *in vitro*, *in vivo* and *ex vivo*. Computer simulation also demonstrated that nanostructures can be considered promising carriers for TO. In addition, all treatments were non-toxic at both the cellular and systemic level. Positively, all substances, in general, present positive results, although the effects observed with rGO were sensibly superior. This nanostructure was able to protect against memory and learning deficits in all behavioral tests performed and had positive effects in decreasing the levels of RS and in AChE activity in the hippocampus. Thus, indicates that this nanostructure is a molecule with multiple targets and can be considered neuroprotective, antioxidant and anticholinesterase. The initial results obtained with this work are promising and stimulate further studies to understand the mechanisms involved in the observed neuroprotective effect. The combination of *in*

silico, in vitro, in vivo and ex vivo reveals a remarkable tool to select out and demonstrating rGO as a promising candidate to be widely investigated in the treatment of Alzheimer's disease.

Authors ethical statement

The manuscript and the data reported here have not been published previously and they are not under consideration for publication elsewhere. All listed authors have contributed significantly to the research and manuscript preparation. They consent to their names on the manuscript, approving thus the final article. All other authors have read the manuscript and have agreed to submit it in its current form for consideration for publication in the *International Journal for Innovation Education and Research.* There is no conflict of interest in the conduct and reporting of research (e.g., financial interests in a test or procedure, funding by pharmaceutical companies for drug research). Animal care and all experimental procedures were conducted in compliance with the National Institutes of Health Guide for the Care and Use of Laboratory Animals (NIH publications no. 80–23, revised in 1996) (National Research Council 1996) and in accordance with the Committee on Care and Use of Experimental Animal Resources, Federal University of Pelotas, Brazil (CEEA 1974/2016). All efforts were made to minimize the number of animals used and their suffering.

CRediT authorship contribution statement

Schopf Patricia Ferreira: Conceptualization, Data curation, Formal analysis, Methodology, Roles/Writing - original draft, Investigation, Visualization. **Pinz Mikaela Peglow:** Conceptualization, Data curation, Formal analysis, Methodology, Roles/Writing - original draft, Investigation, Visualization. **Zanella Ivana:** Resources, Writing - Review & Editing, Validation, Supervision, Funding acquisition. **Wilhelm Ethel Antunes:** Resources, Supervision, Project administration, Funding acquisition. **Luchese Cristiane:** Conceptualization, Resources, Writing - Review & Editing, Validation, Supervision, Project administration, Funding acquisition. **Sagrillo Michele Rorato:** Conceptualization, Resources, Writing - Review & Editing, Validation, Supervision, Project administration, Funding acquisition. **Da Motta Ketlyn Pereira:** Methodology**. Klein Vitor Pereira:** Methodology. **Machado Alencar Kolinski:** Methodology. **Rhoden Cristiano Rodrigo Bohn:** Methodology.

Funding

Declaration of competing interest

The authors declare that they have no known competing financial interests or personal relationships that could have appeared to influence the work reported in this paper.

Acknowledgments

References

Aguiar, J. P. L., 1996. Tabela de composição de alimentos da Amazônia. Acta Amaz. 26, 121-126.

Baldissera, M. D. et al., 2017. Antihyperglycemic, antioxidant activities of tucuma oil (*Astrocaryum vulgare*) in alloxan-induced diabetic mice, and identification of fatty acid profile by gas chromatograph: New natural source to treat hyperglycemia. Chem. Biol. Interact. 270, 51-58. https://doi.org/10.1016/j.cbi.2017.04.001

Bianco, A., 2013. Graphene: Safe or Toxic? The Two Faces of the Medal. Angew. Chem. 52, 4986-4997. https://doi.org/10.1002/anie.201209099

Bermam, H. M. et al., 2000. The protein data bank. Nucleic Acids Res. 28, 235-242. https://doi.org/10.1093/nar/28.1.235

Bony, E. et al., 2012. Awara (*Astrocaryum vulgare* M.) pulp oil: Chemical characterization, and anti-inflammatory properties in a mice model of endotoxic shock and a rat model of pulmonary inflammation. Fitoterapia 83, 33-43. https://doi.org/10.1016/j.fitote.2011.09.007

Bradford, M. M., 1976. A rapid and sensitive method for the quantitation of microgram quantities of protein utilizing the principles of protein-dye binding. Anal. Biochem. 72, 248-254. https://doi.org/10.1016/j.cj.2017.04.003

Butterfield, D. A, Halliwell, B., 2019. Oxidative stress, dysfunctional glucose metabolism and Alzheimer disease. Nat. Rev. Neurosci. 20, 148-160. https://doi.org/10.1038/s41583-019-0132-6

Chen, Y. et al., 2012. Graphene and its derivatives: switching ON and OFF. Chem. Soc. Rev. 41, 4688-4707. https://doi.org/10.1039/C2CS35043B

Cheung, J. et al., 2012. Structures of Human Acetylcholinesterase in Complex with Pharmacologically Important Ligands. J. Med. Chem. 55, 10282-10286. https://doi.org/10.1021/jm300871x

De Rosso, W., Mercadante, A. Z., 2007. Identification and quantification of carotenoids, by HPLC-PDA-MS/MS, from Amazonian fruits. J. Agr. Food Chem. 55, 5062-5072. https://doi.org/10.1021/jf0705421

Dick, M. K.; Limaiem, F., 2019. Histology, Fibroblast. StatPearls, NCBI Bookshelf: Treasure Island.

Dreyer, D. R. et al., 2010. The chemistry of graphene oxide. Chem. Soc. Rev. 39, 228-240. https://doi.org/10.1039/B917103G

Durruthy, M. G. et al., 2017. Decrypting Strong and Weak Single-Walled Carbon Nanotubes Interactions with Mitochondrial Voltage-Dependent Anion Channels Using Molecular Docking and Perturbation Theory. Sci. Rep. 7, 1-19. https://doi.org/10.1038/s41598-017-13691-8

Ellman, G. L. et al., 1961. A new and rapid colorimetric determination of acetylcholinesterase activity. Biochem. Pharmacol. 7, 88-95. https://doi.org/10.1016/0006-2952(61)90145-9

Feinstein, W. P.; Brylinski, M., 2015. Calculating an optimal box size for ligand docking and virtual screening against experimental and predicted binding pockets. J. Cheminformatics 7, 7-18. https://doi.org/10.1186/s13321-015-0067-5

Ferreira, E. S. et al., 2008. Caracterização físico-química do fruto e do óleo extraído de tucumã (*astrocaryum vulgare mart*). Alimentos e Nutrição 19, 427-433.

Forli, S. et al., 2016. Computational protein-ligand docking and virtual drug screening with the AutoDock suite. Nat. Protoc. 11, 905-919. https://doi.org/10.1038/nprot.2016.051

Fraczek-Szczypta, A. Jantas, D. Ciepiela, F. Grzonka, J. Bernasik, A. Marze, Carbon nanomaterials coatings–properties and influence on nerve cells response. Diam Relat Mater, 84 (2018) 127-140. https://doi.org/10.1016/j.diamond.2018.03.017

Fronza, M. G. et al., 2019. Rational design, cognition and neuropathology evaluation of QTC-4-MeOBnE in a streptozotocin-induced mouse model of sporadic Alzheimer's disease. Sci. Rep. 9, 1-14. https://doi.org/10.1038/s41598-019-43532-9

Georgakilas, V., Perman, J. A., Tucek, J., & Zboril, R. Broad family of carbon nanoallotropes: classification, chemistry, and applications of fullerenes, carbon dots, nanotubes, graphene, nanodiamonds, and combined superstructures. Chemical reviews, v. 115, n. 11, p. 4744-4822, 2015. https://pubs.acs.org/doi/full/10.1021/cr500304f

Graham, M. L.; Prescott, M. J., 2015. The multifactorial role of the 3Rs in shifting the harmbenefit analysis in animal models of disease. Eur. J. Pharmacol. 759, 19-29. https://doi.org/10.1016/j.ejphar.2015.03.040

Grieb, P., 2016. Intracerebroventricular Streptozotocin Injections as a Model of Alzheimer's Disease: in Search of a Relevant Mechanism. Mol. Neurobiol. 53, 1741- 1752. https://doi.org/10.1007/s12035-015-9132-3

Guo, X.; Mei, N., 2014. Assessment of the toxic potential of graphene family nanomaterials. J. Food Drug Anal. 22, 105- 115. https://doi.org/10.1016/j.jfda.2014.01.009

Haley, T. J.; Mccormick, W. G., 1957. Pharmacological effects produced by intracerebral injection of drugs in the conscious mouse. Br J Pharmacol. Chemother 12, 12-15. https://doi.org/10.1111/j.1476-5381.1957.tb01354.x

He, Z. et al., 2016. The structural development of primary cultured hippocampal neurons on a graphene substrate. Colloids Surf. B: Biointerfaces 146, 442-451. https://doi.org/10.1016/j.colsurfb.2016.06.045

Jiménez, J. et al., 2017. DeepSite: protein-binding site predictor using 3D-convulation neural networks. Bioinformatics 33, 3036-3042. https://doi.org/10.1093/bioinformatics/btx350

Krishna, I. V. et al., 2009. Cytotoxic studies of anti-neoplastic drugs on human lymphocytes - *In vitro* studies. Cancer Biomark. 5, 261-272. https://doi.org/10.3233/CBM-2009-0111

Laskowski, R. M.; Swindells, M. B., 2011. LigPlot+: Multiple Ligand-Protein Interaction Diagrams for Drug Discovery. J. Chem. Inf. Model. 51, 2778-2786. https://doi.org/10.1021/ci200227u

Lerf, A. et al., 1998. Structure of Graphite Oxide Revisited. J. Phys. Chem. B 102, 4477-4482. https://doi.org/10.1021/jp9731821

Lima, D. A. 2008. Tratamento farmacológico da doença de Alzheimer. Braz. J. Health Biomed. Sci. 7, 78-87.

Loetchutinat, C. et al., 2005. Spectrofluorometric determination of intracellular levels of reactive oxygen species in drug-sensitive and drug-resistant cancer cells using the 2′,7′-dichlorofluorescein diacetate assay. Radiat. Phys. Chem. 72, 323-331. https://doi.org/10.1016/j.radphyschem.2004.06.011

Reina, G., González-Domínguez, J. M., Criado, A., Vázquez, E., Bianco, A., & Prato, M. Promises, facts and challenges for graphene in biomedical applications. Chemical Society Reviews, v. 46, n. 15, p. 4400-4416, 2017. https://pubs.rsc.org/no/content/articlehtml/2017/cs/c7cs00363c

MacKay, E. M.; MacKay, L. L., 1927. The Concentration of Urea in the Blood of Normal Individuals 1. J Clin. Invest. 4, 295-306. https://doi.org/10.1172/jci100124

Martini, F. et al., 2019. A multifunctional compound ebselen reverses memory impairment, apoptosis and oxidative stress in a mouse model of sporadic Alzheimer's disease. J Psychiatr. Res. 109, 107-117. https://doi.org/10.1016/j.jpsychires.2018.11.021

Masoumi, J. et al., 2018. Apelin, a promising target for Alzheimer disease prevention and treatment. Neuropeptides 70, 76-86. https://doi.org/10.1016/j.npep.2018.05.008

Mendonça, M. C. P. et al., 2015. Reduced graphene oxide induces transient blood-brain barrier opening: an in vivo study. J. Nanobiotechnology 13, 1-13. https://doi.org/10.1186/s12951-015-0143-z

Mendonça, M. C. P. et al., 2016. Reduced graphene oxide: nanotoxicological profile in rats. J Nanobiotechnology 14, 1-13. https://doi.org/10.1186/s12951-016-0206-9

Misra, H. P.; Fridovich, I., 1972. The role of superoxide anion in the autoxidation of epinephrine and a simple assay for superoxide dis- mutase. J Biol Chem 247, 3170-3175. http://www.jbc.org/content/247/10/3170

Mokrani, E. H. et al., 2019. Identification of New Potent Acetylcholinesterase Inhibitors Using Virtual Screening and in vitro Approaches. Mol. Inform. 38, 1-11. https://doi.org/10.1002/minf.201800118

Nascimento, K. et al., 2019. Phytochemical analysis and evaluation of the antioxidant and antiproliferative effects of Tucumã oil nanocapsules in breast adenocarcinoma cells (MCF-7). Nat. Prod. Res., 1-6.

National Research Council, 1996. Guide for the Care and Use of Laboratory Animals. The National Academies Press, Washington (DC).

Nobili, A. et al., 2017. Dopamine neuronal loss contributes to memory and reward dysfunction in a model of Alzheimer's disease. Nat. Commun. 8, 1-14.

Ohkawa, H.; Ohishi, N.; Yagi, K., 1979. Assay for lipid peroxides in animal tissues by thiobarbituric acid reaction. Anal. Biochem. 95, 351-358. https://doi.org/10.1016/0003-2697(79)90738-3

Passini, E. et al., 2017. Human In Silico Drug Trials Demonstrate Higher Accuracy than Animal Models in Predicting Clinical Pro-Arrhythmic Cardiotoxicity. Front. Physiol. 8, 1-15. https://doi.org/10.3389/fphys.2017.00668

Pinz, M. P. et al., 2021. Effect of a purine derivative containing selenium to improve memory decline and anxiety through modulation of the cholinergic system and Na^+/K^+-ATPase in an Alzheimer's disease model. Metab. Brain Dis. 36, 871-888. https://doi.org/10.1007/s11011-021-00703-w

Poirier, J., Gauthier, S. 2016. Doença de Alzheimer: o guia completo. São Paulo: MG Editores, 176 p.

Reddy, S. et al., 2018. Allotropic carbon (graphene oxide and reduced graphene oxide) based biomaterials for neural regeneration. Curr. Opin. Biomed. Eng. 6, 120-129. https://doi.org/10.1016/j.cobme.2018.05.001

Reitman, S.; Frankel, S., 1957. A Colorimetric Method for the Determination of Serum Glutamic Oxalacetic and Glutamic Pyruvic Transaminases. Am. J Clin. Pathol. 28, 56-63. https://doi.org/10.1093/ajcp/28.1.56

Rosas, J. J. H. et al., 2011. First principles calculations of the electronic and chemical properties of graphene, graphane, and graphene oxide. J. Mol. Model. 17, 1133-1139. https://doi.org/10.1007/s00894-010-0818-1

Salles, T. R. Rodrigues, H. B. Bruckmann, F. S. Alves, L. C. S. Mortari, S. R. Rhoden, C. R. B, Graphene oxide optimization synthesis for application on laboratory of Universidade Franciscana, Discip. sci., Ser. cienc. nat. tecnol. 21 (2020) 15-26. https://doi.org/10.37779/nt.v21i3.3632

Sakaguchi, M. et al., 2006. Effects of systemic administration of beta-casomorphin-5 on learning and memory in mice. Eur. J. Pharmacol. 530, 81-87. https://doi.org/10.1016/j.ejphar.2005.11.014

Sarter, M.; Bodewitz, G.; Stephens, D. N., 1988. Attenuation of scopolamine induced impairment of spontaneous alternation behavior by antagonist but not inverse agonist and bcarboline. Psychopharmacol. 94, 491-495. https://doi.org/10.1007/BF00212843

Serlin, Y. et al., 2015. Anatomy and Physiology of the Bloond-Brain Barrier. Semin. Cell Dev. Biol. 38, 2-6. https://doi.org/10.1016/j.semcdb.2015.01.002

Servant, A. et al., 2014. Graphene for multi-functional synthetic biology: the last 'zeitgeist' in nanomedicine. Bioorg. Med. Chem. Lett. 24, 1638-1649. https://doi.org/10.1016/j.bmcl.2014.01.051

Shanley, P.; Serra, M.; Medina, G., 2010. Frutíferas e plantas úteis na vida amazônica. 2 ed. Belém: CIFOR, Imazon.

Silveira, C. H. et al., 2009. Protein cutoff scanning: A comparative analysis of cutoff dependent and cutoff free methods for prospecting contacts in proteins. Proteins: Struct., Funct., Bioinf. 74, 727-743. https://doi.org/10.1002/prot.22187

Singh, D. P. et al., 2018. Graphene oxide: An efficient material and recent approach for biotechnological and biomedical applications. Mat. Sci. Eng. C 86, 173-197. https://doi.org/10.1016/j.msec.2018.01.004

Soler, J. M. et al., 2002. The SIESTA method for ab initio order-N materials simulation. Chem. Rev. 14, 2745-2779. https://doi.org/10.1088/0953-8984/14/11/302

Stangherlin, E. C.; Rocha, J. B.; Nogueira, C. W., 2009. Diphenyl ditelluride impairs short-term memory and alters neurochemical parameters in young rats. Pharmacol. Biochem. Behav. 91, 430-435. https://doi.org/10.1016/j.pbb.2008.08.020

Trott, O.; Olson, A. J., 2010. AutoDock Vina: Improving the speed and accuracy of docking with a new scoring function, efficient optimization, and multithreading. J. Comput. Chem. 31, 455-461. https://doi.org/10.1002/jcc.21334

Varadarajan, S. et al., 2001. Different Mechanisms of Oxidative Stress and Neurotoxicity for Alzheimer's $A\beta(1-42)$ and $A\beta(25-35)$. J. Am. Chem. Soc. 123, 5625-5631. https://doi.org/10.1021/ja010452r

Viana, A. R. Salles, B. Bruckmann, F. S. Krause, L. M. F. Mortari, S. R. Rhoden, C. R. B, Cytotoxicity study of graphene oxide against vero lineage cells, Discip. sci., Ser. cienc. nat. tecnol. 20 (2019) 355-364. https://doi.org/10.37779/nt.v20i3.2981

Walsh, R. N.; Cummins, R. A., 1976. The open-field test: a critical review. Psychol. Bull. 83, 482-504. https://doi.org/10.1037/0033-2909.83.3.482

Wang, Y. et al., 2016. Pubchem BioAssay: 2017 update. Nucleic Acids Res. 45, 955-963. https://doi.org/10.1093/nar/gkw1118

Yildirimer, L. et al., 2011. Toxicology and clinical potential of nanoparticles. Nanotoday 6, 585-607. https://doi.org/10.1016/j.nantod.2011.10.001

Yuyama, L. K. O. et al., 2008. Processing and evaluation of the shelf-life of tucumã (Astrocaryum aculeatum Meyer) dehydrated and pulverized. Technological Science food. 28, 408-412. https://doi.org/10.1590/S0101-20612008000200021